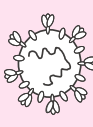
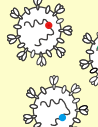
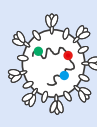

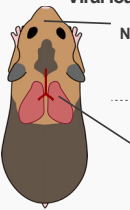

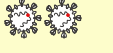
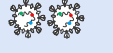





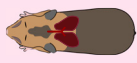
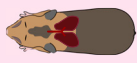








Article

Versatile live-attenuated SARS-CoV-2 vaccine platform applicable to variants induces protective immunity

	Wild type virus	Temperature-sensitive mutants	Engineered temperature-sensitive virus	Versatile live-attenuated vaccine platform
				
		Mutagenesis	CPER recombination	Spike exchange in 2 weeks
Proliferation at 37°C	+++	+ / -	-	-
 Viral load Nasal cavity Lungs	 +++	 ++	 ++	 ++
	 +++	 +	 +	 +
Risk of virulence reversion	Not applicable	High	Low	Low
Pathogenicity  Tissue damage Weight decrease				
		No weight decrease	No weight decrease	No weight decrease
 Nasal wash nAb titer  Serum nAbs Titer  Persistence	+++	Not determined	+++	Not determined
	+++	+++	+++	+++
	Not determined	Maintained for up to 4 months	Not determined	Not determined

Akiho Yoshida, Shinya Okamura, Shiho Torii, ..., Shiro Takekawa, Koichi Yamanishi, Hirotaka Ebina

hebina@biken.osaka-u.ac.jp

Highlights

Temperature-sensitive CoV-2 with mutations in *nsp3*, *nsp14*, and *nsp16* were isolated

Combination of these mutations led to reduced risk of virulent reversion

Engineered viral strain showed strong immunogenicity *in vivo*

A live-attenuated vaccine platform with exchangeable spike protein was established

Yoshida et al., iScience 25, 105412
November 18, 2022 © 2022 The Authors.
<https://doi.org/10.1016/j.isci.2022.105412>

Article

Versatile live-attenuated SARS-CoV-2 vaccine platform applicable to variants induces protective immunity

Akiho Yoshida,^{1,2,7} Shinya Okamura,^{1,2,7} Shiho Torii,^{3,4} Sayuri Komatsu,^{1,2} Paola Miyazato,^{1,2} Hitomi Sasaki,² Shiori Ueno,⁵ Hidehiko Suzuki,^{1,2} Wataru Kamitani,⁵ Chikako Ono,^{3,4} Yoshiharu Matsuura,^{3,4} Shiro Takekawa,² Koichi Yamanishi,² and Hirotaka Ebina^{1,2,6,8,*}

SUMMARY

Live-attenuated vaccines are generally highly effective. Here, we aimed to develop one against SARS-CoV-2, based on the identification of three types of temperature-sensitive (TS) strains with mutations in nonstructural proteins (nsp), impaired proliferation at 37°C–39°C, and the capacity to induce protective immunity in Syrian hamsters. To develop a live-attenuated vaccine, we generated a virus that combined all these TS-associated mutations (rTS-all), which showed a robust TS phenotype *in vitro* and high attenuation *in vivo*. The vaccine induced an effective cross-reactive immune response and protected hamsters against homologous or heterologous viral challenges. Importantly, rTS-all rarely reverted to the wild-type phenotype. By combining these mutations with an Omicron spike protein to construct a recombinant virus, protection against the Omicron strain was obtained. We show that immediate and effective live-attenuated vaccine candidates against SARS-CoV-2 variants may be developed using rTS-all as a backbone to incorporate the spike protein of the variants.

INTRODUCTION

The COVID-19 pandemic, caused by the pathogen SARS-CoV-2, has had a serious impact on public health, with more than 500 million infection cases and over six million deaths reported worldwide (ourworldindata.org). To prevent the spread of COVID-19, several adenovirus-vectored and mRNA vaccines encoding the viral spike (S) protein gene have been developed and are presently widely used. These vaccines have been reported to induce robust humoral and cellular immune responses ([Folegatti et al., 2020](#); [Jackson et al., 2020](#); [Sahin et al., 2021](#)); however, there are concerns regarding adverse reactions caused by these vaccines, such as thrombosis and fever. Furthermore, variants of concern (VOC), which bear several mutations in the S protein, continually arise and contribute to the evasion of the humoral immunity generated against the ancestral S protein ([Baum et al., 2020](#); [Edara et al., 2021](#); [Wibmer et al., 2021](#)). To increase the induction of neutralizing antibodies against VOCs, such as the SARS-CoV-2 Omicron variant, most countries have been encouraging a third, and even a fourth, vaccine dose as a booster. Nevertheless, the antibody response induced by these vaccines is not persistent, demanding the development of alternative vaccines of different modalities to better control the ongoing pandemic.

Traditional live-attenuated vaccines are highly effective and have been successfully used against various diseases, including varicella, measles, and rubella viruses. These vaccines were developed by heterogeneous adaptation, isolating mutant viruses that cannot propagate in human cells ([Makino et al., 1970](#); [Parks et al., 2001](#); [Sasaki, 1974](#); [Shishido and Ohtawara, 1976](#); [Takahashi et al., 1974](#); [Zimmerman et al., 2018](#)), or by isolating temperature-sensitive (TS) viruses that cannot replicate at the physiological human body temperature ([Komase et al., 2006](#); [Okamoto et al., 2016](#)). In addition, a live influenza virus vaccine was developed by reassortment of viruses generated from a cold-adapted donor virus with temperature sensitivity-related mutations in six vRNA segments ([Maassab and Bryant, 1999](#); [Murphy and Coelingh, 2002](#)). The attenuated phenotype of this virus was confirmed by its capacity to replicate at 25°C–33°C but not at 37°C ([Cox and Dewhurst, 2015](#)). Therefore, several groups have been developing live-attenuated vaccines against SARS-CoV-2. For example, Trimpert et al. and CODAGENIX are developing a codon

¹Virus Vaccine Group, BIKEN Innovative Vaccine Research Alliance Laboratories, Institute for Open and Transdisciplinary Research Initiatives, Osaka University, Suita, Osaka, Japan

²The Research Foundation for Microbial Diseases of Osaka University, Suita, Osaka, Japan

³Laboratory of Virus Control, Research Institute for Microbial Diseases, Osaka University, Suita, Osaka, Japan

⁴Laboratory of Virus Control, Center for Infectious Disease Education and Research, Osaka University, Suita, Osaka, Japan

⁵Department of Infectious Diseases and Host Defense, Gunma University Graduate School of Medicine, Maebashi, Gunma, Japan

⁶Virus Vaccine Group, BIKEN Innovative Vaccine Research Alliance Laboratories, Research Institute for Microbial Diseases, Osaka University, Suita, Osaka, Japan

⁷These authors contributed equally

⁸Lead contact

*Correspondence: hebina@biken.osaka-u.ac.jp
<https://doi.org/10.1016/j.isci.2022.105412>



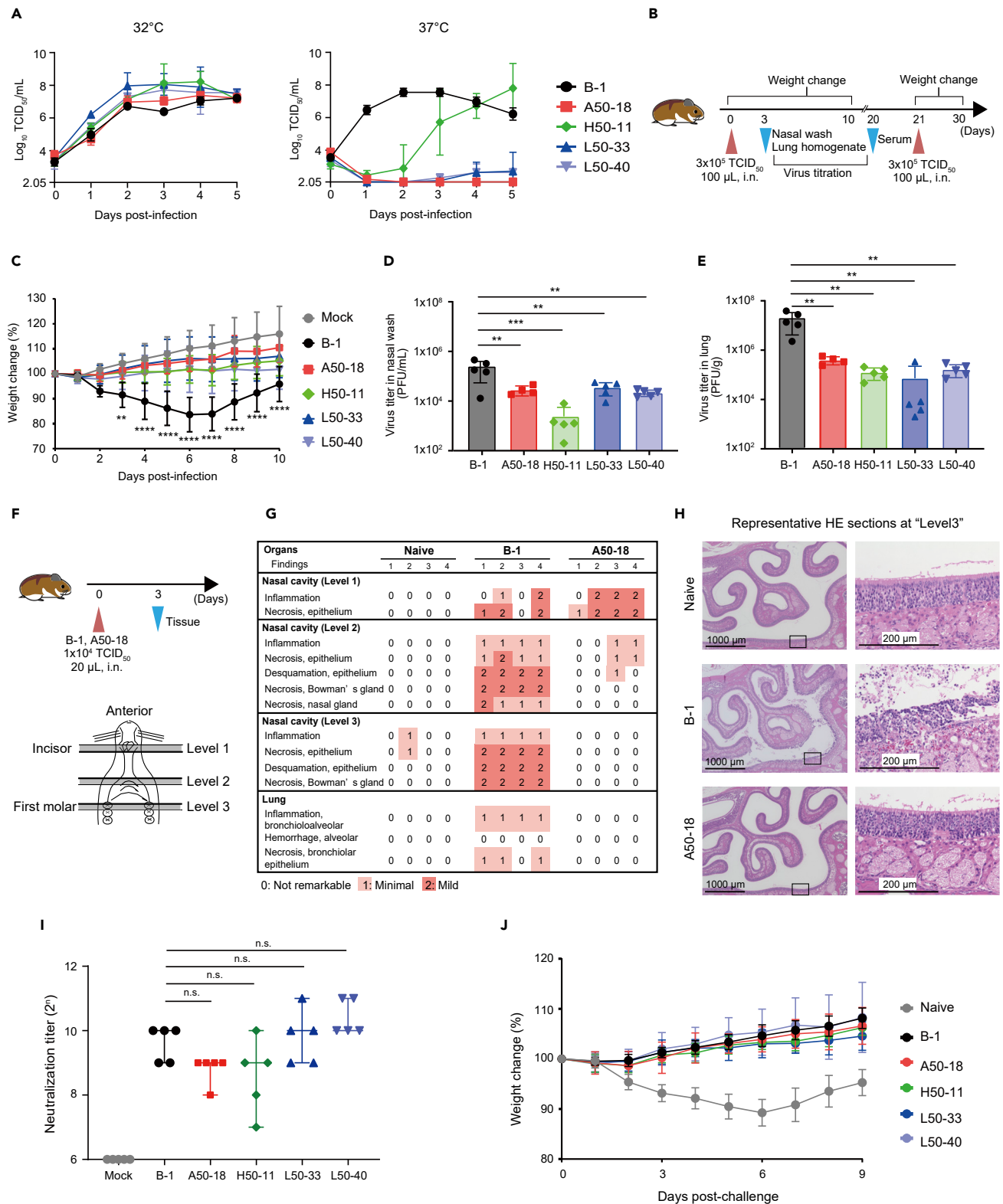


Figure 1. SARS-CoV-2 TS mutants show attenuated phenotype and induce protective immunity

(A) Comparison of the growth kinetics of the four TS mutants with those of the B-1 strain at different temperatures. Vero cells were infected with each strain at multiplicity of infection (MOI) = 0.01. The viral titer of the supernatant was evaluated by TCID₅₀ using Vero cells. Symbols represent the average of three

Figure 1. Continued

independent experiments, and error bars depict the mean SDs. For samples below the limit of detection (LOD), the assay's LOD was used to calculate the mean. The LOD is $2.05 \log_{10}$ TCID₅₀/mL, indicated in the x-axis. TCID₅₀: 50% tissue culture infectious dose. To compare titers on the same day between the B-1 and the other strains, two-way ANOVA was performed.

(B) Overview of the evaluation for pathogenicity and immunogenicity of TS mutants (n = 5).

(C) Weight changes in the Syrian hamsters infected with the TS mutant or B-1 strains. The average weight change is plotted, and error bars represent the SDs. To compare weight change on the same day between the mock and the other groups, two-way ANOVA was performed (**p < 0.01 and ****p < 0.0001).

(D and E) The viral titers of nasal wash specimens (D) and lung homogenates (E) three days post-infection. Infectious viruses were evaluated by plaque formation assays. PFU: plaque-forming units. Bars depict the mean values, and symbols represent individual viral titers. Error bars represent SDs. For statistical analysis, one-way ANOVA was performed (**p < 0.01 and ***p < 0.001).

(F) Schematic diagram for the evaluation of mucosal tissue damage (n = 4).

(G) Damage scores of each section. The percentage of the disrupted area in the entire visual field was classified as 0: not remarkable (< 10%), 1: minimal (10%–50%), and 2: mild (50%–70%), respectively.

(H) Representative hematoxylin and eosin (HE)-stained images of sections at level 3. Scale bar: 1000 μ m (left panel), and 200 μ m (right panel). Right panels are higher magnification images of the marked areas.

(I) Neutralization titers of the sera from hamsters infected with each strain and mock-treated hamsters. Median values are plotted, and error bars represent the 95% CIs. For statistical analysis, the Kruskal-Wallis test was performed (n.s.: not significant). The LOD is indicated in the x-axis.

(J) Weight change in hamsters after B-1 virus reinfection. The average weight change is plotted, and error bars represent mean SDs. To compare weight change on the same day between the naive and the other groups, two-way ANOVA was performed.

deoptimization strategy (Trimpert et al., 2021; Wang et al., 2021) and Seo et al. followed the cold-adaptation approach for isolating live-attenuated TS strains (Seo and Jang, 2020).

In this study, we obtained four TS SARS-CoV-2 strains from a clinical isolate by random mutagenesis. These strains exhibited low pathogenicity and protecting immunogenicity *in vivo*. We identified that mutations in *nsp3*, *nsp14*, and *nsp16* genes are associated with the TS phenotype and generated a highly effective and safe live-attenuated vaccine candidate by combining these TS-related mutations. Moreover, this candidate vaccine could be adjusted with an appropriate S protein to generate vaccines for specific VOCs. We believe that this live-attenuated vaccine candidate is a promising platform to control the spread of the COVID-19 pandemic.

RESULTS**SARS-CoV-2 TS mutants show attenuated phenotype and induce protective immunity**

To isolate the TS strains of SARS-CoV-2, we generated a library of viruses containing random mutations from the clinical isolate B-1 virus (accession number: LC603286) (Figure S1A). In total, 659 viral plaques were isolated from the library and screened. Vero cells were infected with all viral clones, cultured at 32°C or 37°C, and monitored daily for cytopathic effects (CPE). During this process, we selected four TS strains that induced CPE at 32°C three days post-infection (dpi) but not at 37°C.

To comprehensively analyze temperature sensitivity, we evaluated the growth kinetics of the isolated TS strains at 32°C, 34°C, and 37°C (Figures 1A and S1B). Under 32°C and 34°C culture conditions, all TS strains replicated comparably to the parent B-1 virus. However, at 37°C, the replication of all TS strains was relatively slower or smaller in scale than that of the parent strain. The growth of the H50-11 strain was delayed (p < 0.001, at day 1); however, its titer on day three was comparable to the viral titer of the B-1 virus on the same day (p = 0.5034). The L50-33 and L50-40 strains slightly proliferated at 37°C, and the viral titers were less than 10⁴ TCID₅₀/mL, even at five dpi, and were 10⁴ times lower than the maximum titer of the B-1 strain. Interestingly, the A50-18 strain showed a unique phenotype, as no infectious viruses were detected in the culture medium at 37°C (the TCID₅₀ was under the assay's limit of detection).

Next, we evaluated the pathogenicity of TS mutant strains in Syrian hamsters, which are widely used as a model for SARS-CoV-2 infection (Imai et al., 2020; Sia et al., 2020) (Figure 1B). Viral pathogenicity was monitored based on the changes in body weight after viral infection. Compared to the mock group, B-1-infected hamsters significantly decreased their body weight, with an approximate decrease of 15% at day six (Figure 1C). In contrast, no body weight loss was observed after infection with any of the tested TS strains. To determine the acute signs that can be observed after infection with the TS strains, B-1- or TS strain-infected Syrian hamsters were euthanized at three dpi, and lung tissue damage was evaluated. The lungs of the B-1-infected hamsters were heavier than those of the mock- or TS-infected hamsters (Figure S1C). Additionally, we observed apparent bleeding and destruction of the alveoli in the lungs of B-1-infected hamsters (Figure S1D). However, we did not observe evident critical tissue damage in the TS-infected hamsters. We also

measured the amount of virus remaining in the nasal cavity and lungs at three dpi. The viral titer in the nasal wash specimens of the TS-infected hamsters was significantly lower than that of the B-1-infected hamsters (Figure 1D). The mean viral titers were 2.25×10^5 , 2.84×10^4 , 2.42×10^3 , 3.57×10^4 , and 2.14×10^4 PFU/mL in B-1-, A50-18-, H50-11-, L50-33-, and L50-40-infected hamsters, respectively. In addition, the viral titer in the lungs of the TS-infected hamsters was approximately 100 times lower than that in the lungs of the B-1-infected group; the mean titers were 1.87×10^7 , 3.98×10^5 , 1.26×10^5 , 7.25×10^4 , and 1.66×10^5 PFU/g in B-1-, A50-18-, H50-11-, L50-33-, and L50-40-infected hamsters, respectively (Figure 1E). These results suggest that the attenuated phenotype of the TS strains was due to impaired viral replication in the lungs. Moreover, to examine whether infection with the TS strains injures the nasal mucosa, we analyzed transverse cross-sections of the nasal cavity at three dpi (Figure 1F). In the “level 1” section, the anterior sections of the nasal cavity, the mucosal damage observed in A50-18-infected hamsters was similar to that observed in B-1-infected hamsters (Figure 1G). However, in “level 2 and 3” slices (medial and posterior sections, respectively), the tissue damage caused by A50-18 infection was milder than that caused by B-1 (Figure 1H), suggesting that intranasal infection with TS strains hardly injures the inner area of the nasal cavity.

To evaluate whether the attenuated TS strains could be used as live vaccines, we measured neutralizing titers in sera collected 20 days after the first infection (Figure 1B). The neutralizing antibody titer was <64, 512–1024, 256–512, 128–1024, 512–2048, and 1024–2048 in the sera of hamsters infected with the mock, B-1, A50-18, H50-11, L50-33, and L50-40 strains, respectively (Figure 1I). To assess the persistence of immunity against the TS strain, we performed a longitudinal analysis of hamsters after A50-18 infection (Figure S1E). Neutralizing antibody titers increased by week 4 and were relatively maintained for at least 16 weeks (Figure S1F). Median titer values were 256, 2048, 724.1, 512, 256, 512, 181, and 256 at weeks 2, 4, 6, 8, 10, 12, 14, and 16, respectively. Additionally, to assess vaccine efficacy, immunized Syrian hamsters were reinfected with the wild-type B-1 virus 21 days after the first infection (Figure 1B). No significant body weight decrease was observed in hamsters pre-infected with B-1 or TS strains, whereas primary B-1 strain infection resulted in noticeable body weight loss in naive hamsters ($p < 0.001$, all groups, days 3 to 9, compared to naive group) (Figure 1J), suggesting the induction of protective immunity. These results indicate that the four attenuated TS strains can be used as live vaccines.

The substitutions nsp3 445F, nsp14 248V plus 416S, and nsp16 67I are crucial for the TS phenotype

We then performed a deep sequencing analysis to identify mutations in the four TS strains (Table 1). The A50-18 strain had six missense mutations in the genes encoding nsp14, S, envelope (E), and nucleocapsid (N) proteins. The H50-11 strain had four missense mutations in the *nsp3*, *nsp16*, and *spike* genes. There were two missense mutations in the *nsp3* gene of the L50-33 strain and three missense mutations in the *nsp3* and *spike* genes of the L50-40 strains. The H50-18, L50-33, and L50-40 strains had a common deletion in *orf7a-orf8* (27549–28251).

To identify TS-related mutations in these TS strains, we sought to obtain revertants of these viruses that can proliferate under high-temperature conditions (37°C–39°C). Vero cells were infected with each of the TS strains at a high multiplicity of infection (MOI; MOI = 1.0) and incubated at 37°C, 38°C, or 39°C. For the A50-18 strain, the number of CPE-positive wells was 19 out of 230 analyzed wells at 37°C and 5 out of 223 wells at 38°C. Sequencing analysis revealed that A50-18 revertants replaced the 248V or 416S substitutions in nsp14 with the wild-type sequence (248G or 416G) but not the other amino acid substitutions (Table 2). Additionally, these revertant viruses proliferated at high temperatures when either of the two substitutions returned to the wild-type amino acid, indicating that the substitutions nsp14 248V and 416G are coordinately involved in the TS phenotype. We compared the predicted crystal structures of A50-18 nsp14 to those of B-1 using AlphaFold2 (Jumper et al., 2021). The model suggested that both 248V and 416S are located near the zinc finger2 domain, which has been reported to be important for enzymatic activity (Figure S2A). The 248V substitution prevented the formation of one hydrogen bond, whereas 416S altered the angle of the other. We obtained H50-11 revertants in 2/230 wells at 37°C and in 1/230 wells at 38°C. In these viruses, the nsp16 67I substitution was changed to the wild-type amino acid (67V) (Table 2). The crystal structure models predicted that the V67I substitution did not significantly affect the structure of nsp16 (Figure S2B). L50-33 revertants were obtained in 34/230 wells at 37°C, 39/228 wells at 38°C, and 13/230 wells at 39°C. L50-40 revertants were obtained in 17/230 wells at 37°C, 14/228 wells at 38°C, and 4/216 wells at 39°C (Table 2). The number of wells that produced L50 revertant viruses was higher than that for the A50-18 and H50-11 strains. In the revertants of L50-33 and L50-40, nsp3 445F changed back to the wild-type amino acid (leucine)

Table 1. Genetic mutation and amino acid substitution in the TS strains

Strain	Genetic mutation	Protein	Amino acid substitution
A50-18	G18782T	nsp14	G248V
	G19285A		G416S
	C19550T		A504V
	C24198T	Spike	A879V
	T26327C	Envelope	L28P
	C28278T	Nucleocapsid	S2F
H50-11 ^a	T3930C	nsp3	V404A
	G8213A		D1832N
	G20857A	nsp16	V67I
	C23778A	Spike	T739K
L50-33 ^a	C4052T	nsp3	L445F
	A8094G		K1792R
L50-40 ^a	C4052T	nsp3	L445F
	A8094G		K1792R
	T21723G	Spike	L54W

^aH50-11, L50-33, L50-40 strains had a common deletion in *orf7a-orf8* (27549-28251).

as expected, or was altered to cysteine, valine, or isoleucine (Table 2). Taken together, these results suggest that nsp14 248V plus 416S, nsp3 445F, and nsp16 67I are responsible for the TS phenotype of each strain.

The phenotype and attenuation of the TS strains are attributed to the substitutions nsp14 248V plus 416S, nsp3 445F, and nsp16 67I

To confirm the role of the identified substitutions in the TS phenotype, we constructed recombinant viruses using a circular polymerase extension reaction (Torii et al., 2021) (Figure 2A). Recombinant viruses bearing the 248V and/or the 416S substitutions in the nsp14 protein (r14_{248V}, r14_{416S}, and r14_{248V, 416S}, respectively), the 67I substitution in the nsp16 (r16_{67I}), the 445F substitution in the nsp3 (r3_{445F}), and the deletion in the *orf7a-orf8* (rΔORF7a-8) were generated. *In vitro* growth kinetics (Figure 2B) and *in vivo* pathogenicity (Figures 2C and 2D) of the viruses were compared. Under the 32°C culture condition, all recombinant mutants (r3_{445F}, r16_{67I}, r14_{248V}, r14_{416S}, r14_{248V, 416S}, and rΔORF7a-8) replicated comparably to the recombinant B-1 (rB-1) strain (Figure 2B). The r14_{248V} and r14_{416S} mutants proliferated comparably to rB-1 at 37°C, whereas r14_{248V, 416S} showed relatively slower growth at 37°C ($p < 0.001$, at day 1, compared to rB-1), and this difference was more pronounced at 39°C. The replication of r14_{248V, 416S} was not detected at 39°C (the TCID₅₀ was under the assay's limit of detection), whereas that of r14_{248V} was slightly delayed ($p < 0.1$, at day 1, compared to rB-1). In contrast, the replication of r14_{416S} was not affected at 39°C. These results suggest that a double amino acid substitution in nsp14 (248V and 416S) is necessary for a stronger TS phenotype, which can be observed at 37°C. The proliferation of the r3_{445F} virus was relatively slower or smaller in scale than that of rB-1 at 37°C ($p < 0.01$, at day 1). Moreover, at 39°C, the replication of these mutants was not detected (the TCID₅₀ was under the assay's limit of detection), indicating that the 445F substitution in nsp3 is responsible for the TS phenotype. The r16_{67I} virus proliferated comparably to rB-1 at 37°C; however, the peak in viral growth at 39°C was delayed two days compared to that of rB-1. These results suggest that the 67I substitution in nsp16 is responsible for the TS phenotype. Similarly, replication of rΔORF7a-8, which is a recombinant mutant with a deletion in *orf7a-orf8* common to H50-11, L50-33, and L50-40, was delayed two days compared to that of rB-1 at 39°C. This result suggests that this deletion negligibly accounts for the TS phenotype. The A50-18 strain has an A504V substitution in nsp14 in addition to G248V and G416S. This triple amino acid substitution impaired plaque formation at 37°C, even at day 6 (Figure S3), suggesting that nsp14 504V is also involved in temperature sensitivity, although it is unnecessary.

Next, we assessed whether these recombinant TS mutants were as attenuated *in vivo* as the isolated parental TS strains, using Syrian hamsters (Figure 2C). A significant decrease in body weight of approximately 15% was observed at six dpi in rB-1-infected hamsters ($p < 0.0001$, compared to the mock group) (Figure 2D). In contrast, no body weight loss was observed after infection with the r3_{445F} or r14_{248V, 416S}

Table 2. Amino acid substitutions in the revertants

37°C					38°C				39°C			
Parent TS strain	Revertants ^a	Amino acid substitution	Codon change	Rate ^b	Revertants ^a	Amino acid substitution	Codon change	Rate ^b	Revertants ^a	Amino acid substitution	Codon change	Rate ^b
A50-18	19/230	nsp14 248G	GTG>GGT	6/19	5/223	nsp14 416G	AGT>GGT	5/5	0/230	–	–	–
		nsp14 416G	AGT>GGT	13/19								
H50-11	2/230	nsp16 67V	ATT>GTT	2/2	1/240	nsp16 67V	ATT>GTT	1/1	0/237	–	–	–
L50-33	34/230	nsp3 445L	TTT>CTT	4/34	39/228	nsp3 445L	TTT>CTT	2/39	13/230	nsp3 445L	TTT>CTT	2/13
			TTT>TTG	17/34			TTT>TTG	22/39			TTT>TTG	6/13
			TTT>TTA	1/34			TTT>TTA	3/39			TTT>TTA	1/13
		nsp3 445C	TTT>TGT	8/34		nsp3 445C	TTT>TGT	7/39		nsp3 445C	TTT>TGT	2/13
		nsp3 445V	TTT>GTT	3/34		nsp3 445V	TTT>GTT	3/39		nsp3 445V	TTT>GTT	2/13
		nsp3 445I	TTT>ATT	1/34		nsp3 445I	TTT>ATT	2/39				
L50-40	17/230	nsp3 445L	TTT>CTT	2/17	14/228	nsp3 445L	TTT>CTT	2/14	4/216	nsp3 445L	TTT>CTT	2/4
			TTT>TTG	9/17			TTT>TTG	9/14			TTT>TTG	1/4
		nsp3 445C	TTT>TGT	6/17		nsp3 445C	TTT>TGT	3/14		nsp3 445C	TTT>TGT	1/4

^aNumber of wells with revertants/Total.

^bRate of wells containing viruses with the specified codon changes.

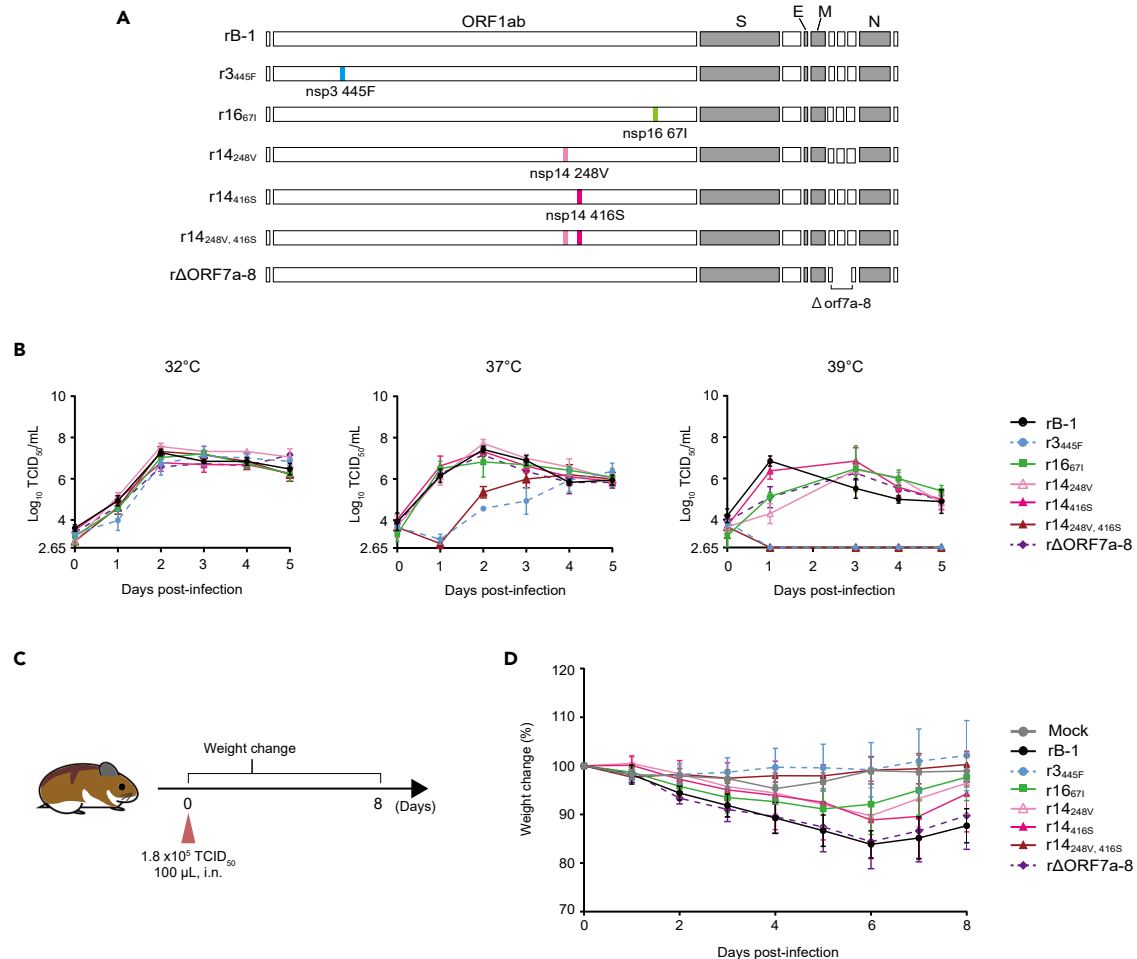


Figure 2. The phenotype and attenuation of the TS strains are attributed to the substitutions nsp14 248V plus 416S, nsp3 445F, and nsp16 671
(A) The construct of recombinant viruses bearing the substitutions or the deletion found in the TS strains.

(B) The growth kinetics of recombinant viruses at different temperatures. Vero cells were infected with each strain at MOI = 0.01. The viral titer of the supernatant was calculated by TCID₅₀ using Vero cells. Symbols represent the average of three independent experiments, and error bars mean SDs. For samples below the LOD, the assay's LOD was used to calculate the mean. The LOD is 2.65 log₁₀ TCID₅₀/mL, indicated in the x axis. To compare titers on the same day between the B-1 and the other strains, two-way ANOVA was performed.

(C) Evaluation of the pathogenicity of recombinant viruses *in vivo* (n = 5).

(D) Weight change in the Syrian hamsters infected with the recombinant viruses. The average weight changes are represented by symbols, and SDs are represented by error bars. For statistical analysis, two-way ANOVA was performed.

viruses ($p > 0.9999$ and $p > 0.9999$, respectively, at day 6, compared to the mock group). The r14_{248V}-, r14_{416S}-, and r16₆₇₁-infected groups showed a decrease in body weight of approximately 10%; however, it was slightly less than that observed in the rB-1-infected group ($p = 0.3308$, $p = 0.6894$, and $p = 0.1592$, respectively, at day 6, compared with rB-1-infected group). The rΔORF7a-8-infected group lost as much weight as the rB-1-infected group did. Therefore, considering the *in vitro* growth kinetics data, the temperature sensitivity of the mutants was consistent with their level of attenuation.

The rTS-all vaccine candidate strain is highly attenuated and shows high immunogenicity in Syrian hamsters

As described above, the TS-associated substitutions changed back to the wild-type amino acid when the virus was found to proliferate at high temperatures (Table 2). Moreover, hamsters infected with the L50-33 revertant exhibited a decrease of approximately 21% in body weight at six dpi (Figure S4A), suggesting a risk of virulent reversion if TS strains are used as vaccines. To decrease the risk of virulent reversion and to generate a safe vaccine candidate, we combined the TS-associated mutations of *nsp3*, *nsp14*, *nsp16*, and

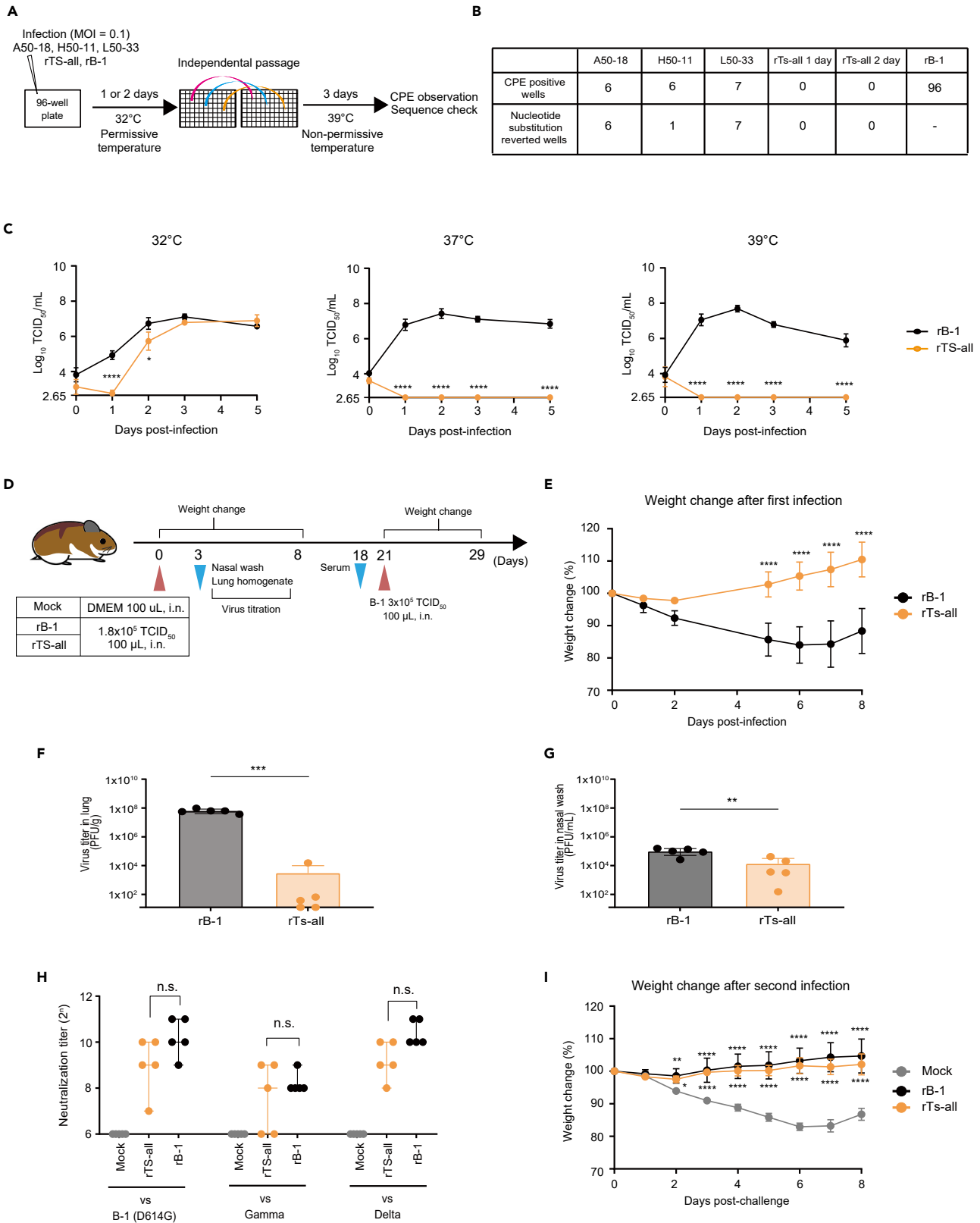


Figure 3. The rTS-all vaccine candidate strain is highly attenuated and shows high immunogenicity in Syrian hamsters

- (A) Scheme for the evaluation of the risk of virulent reversion by their ability to replicate at lower temperatures.
- (B) The number of CPE-positive wells (upper line) and that of those that changed back to the wild-type sequence (lower line).
- (C) Growth dynamics of the rTS-all and rB-1 strains at different temperatures. Vero cells were infected with each strain at MOI = 0.01. Infectious viruses in the supernatants were evaluated by TCID₅₀ in Vero cells. Symbols represent the average of three independent experiments, and error bars represent SDs. For samples below the LOD, the assay's LOD was used to calculate the mean. The LOD is 2.65 log₁₀ TCID₅₀/mL, indicated in the x axis. For statistical analysis, two-way ANOVA was performed (*p < 0.05, ****p < 0.0001).
- (D) Overview of the investigation of the pathogenicity and immunogenicity of the rTS-all strain (n = 5).
- (E) Weight change in the recombinant viruses-infected hamsters. The average weight change is plotted, and error bars represent the SDs. For statistical analysis, two-way ANOVA was performed (****p < 0.0001).
- (F and G) The viral titers in lung homogenates (F) and nasal wash specimens (G) three days post-infection. Viral titration was performed by plaque formation assays. Bars depict the mean values, and symbols represent individual viral titers. Error bars represent mean SDs. The LOD is indicated in the x axis. For statistical analysis, one-way ANOVA was performed (**p < 0.01 and ***p < 0.001).
- (H) Neutralization titers in the sera of rB-1 or rTS-all-infected and mock-treated hamsters. Symbols represent individual neutralization titers. Bars show median values and error bars represent 95% CIs. For statistical analysis, the Kruskal-Wallis test was performed (n.s.: not significant). The LOD is indicated in the x axis.
- (I) Weight change in Syrian hamsters after reinfection with the B-1 virus. The average weight change is plotted, and error bars represent mean SDs. To compare weight change on the same day between the naïve and the other groups, two-way ANOVA was performed (*p < 0.05, **p < 0.01, and ****p < 0.0001).

Δorf7a-orf8, whose mechanisms were predicted to be independent of one another (rTS-all). Thus, these mutations may act in synergy or complement each other, rendering a more stable TS phenotype. To assess the reversion risk of rTS-all, we performed the experiment described in Figure 3A. Each TS virus was transferred to 39°C culture conditions, a non-permissive temperature, after an incubation period of one or two days at 32°C. Three days after passaging, we counted the number of CPE-positive wells and checked the genomic sequence of the TS-responsible substitutions of viruses in these wells. Replication of the B-1 strain was observed in all wells (Figure 3B). In contrast, no CPE-positive wells were detected in the rTS-all-inoculated wells, whereas several revertants were detected in the isolated TS strains (A50-18, H50-11, and L50-33). Moreover, to confirm whether the rTS-all reverts its amino acid substitution and recovers its virulence *in vivo*, hamsters were infected with rTS-all or L50-33 strains, and the genomic viral sequences and titers in nasal wash specimens were analyzed (Figure S4B). Although none of the infected hamsters lost weight (Figure S4C), the virus titer in nasal wash specimens of L50-33-infected hamsters was higher than that of rTS-all-infected hamsters (Figure S4D). Consistently, these viruses showed sequence alterations encoding for most probably leucine or cysteine at position 445 in nsp3, showing no TS phenotype (Figure S4D, Table 2). In contrast, rTS-all did not show changes in any of the TS mutations, in three independent experiments (Figure S4E). These results suggest that the risk of virulent reversion of rTS-all might be lower than that of the isolated TS strains. Furthermore, the *in vitro* growth kinetic assays demonstrated that the replication of rTS-all was impaired under 37°C and 39°C culture conditions (Figure 3C). Even at 32°C, rTS-all started to proliferate later than rB-1, at one dpi (p < 0.0001). These results suggest that rTS-all is highly sensitive to temperature.

To investigate the *in vivo* levels of attenuation and immunogenicity, Syrian hamsters were first inoculated intranasally with 1.8×10^5 TCID₅₀/100 μL/dose of rB-1 or rTS-all and reinfected with the wild-type B-1 virus 21 days later (Figure 3D). No body weight loss was observed after primary infection with rTS-all; however, the body weight of the rB-1-infected group decreased by approximately 15%, suggesting that rTS-all was indeed attenuated (Figure 3E). Moreover, the viral titer in the lungs of rTS-all-infected hamsters was remarkably lower than that in the lungs of rB-1-infected hamsters, with mean viral titers of 6.29×10^7 and 3.08×10^3 PFU/g in rB-1- and rTS-all-infected hamsters, respectively (Figure 3F). The viral titer in nasal wash specimens of rTS-all-infected hamsters was also markedly lower than that of rB-1-infected hamsters, with mean viral titers of 1.01×10^5 and 1.39×10^4 PFU/mL in rB-1- and rTS-all-infected hamsters, respectively (Figure 3G). These results indicated that rTS-all is a hyper-attenuated mutant as its replication in the lungs is greatly impaired.

The titer of neutralizing antibodies in the serum of mock-infected hamsters was <64 (Figure 3H), and it was not significantly different between the rTS-all-infected group and the rB-1-infected group, ranges being 128–1024 (vs B-1), 64–512 (vs Gamma strain: hCoV-19/Japan/TY7-501/2021), and 256–1024 (vs Delta strain: BK325), respectively. These results suggest that the humoral immune responses induced by infection with the attenuated rTS-all were comparable to that induced by rB-1, even against heterologous virus infection. Importantly, no significant weight decrease was observed after challenging hamsters

pre-infected with rB-1 or rTS-all with the B-1 virus (Figure 3I), suggesting that infection with rTS-all induced protective immunity.

Live-attenuated TS viruses are effective against the variant Omicron

Antigenic drift has enabled Omicron, the latest VOC, to propagate around the world and become dominant in one month, according to [COVID Data Tracker](#). To evaluate whether rTS-all-infection protects against the Omicron variant, Syrian hamsters were inoculated intranasally with 1.8×10^5 TCID₅₀/100 μ L/dose of rB-1 or rTS-all. Inoculation with rB-1 and rTS-all induced neutralizing antibodies against the homologous virus B-1 (Figure 4B). Furthermore, titers against the Omicron variant were <32–128 in hamsters infected with rB-1 or rTS-all (Figure 4C). To evaluate whether rTS-all induces heterologous protection, animals were challenged with the TY38-873 Omicron virus (7.2×10^4 TCID₅₀/20 μ L) 28 days after the initial inoculation (n = 5, Figure 4A). Viral titers in the lungs and nasal specimens, collected three days after Omicron infection, were measured by plaque assays. In the lungs, the mean viral titer in the rB-1- and rTS-all-infected groups was significantly lower than that in the mock-infected group, which had a titer of 6.4×10^5 PFU/g (Figure 4D). The mean viral titer in nasal wash specimens of the rB-1- and rTS-all-infected groups was remarkably lower than that of the mock-infected group (5.2×10^3 PFU/mL; Figure 4E). Additionally, the titers in the lungs and nasal wash of the rB-1- and rTS-all-infected groups were not significantly different, suggesting that rTS-all infection can protect hamsters from an Omicron infection, as well as the wild-type infection, by inducing cross-reactive neutralizing antibodies. Moreover, we compared the neutralizing antibody titers in the nasal wash specimens of the rB-1- and rTS-all-infected groups, collected 28 days after primary infection, using a VSV Δ G/Luc-encoding SARS-CoV-2 S-expressing pseudovirus (Tani et al., 2010). The nasal wash specimens of the rTS-all-infected group showed significantly lower luciferase activity than that of the mock group, similar to the rB-1-infected group (Figure 4F). This result suggests that infection of the nasal mucosa with rTS-all can induce neutralizing antibodies to protect against viral entry. Collectively, these data demonstrate that infection with rTS-all induces the production of systemic and mucosal neutralizing antibodies, which can prevent infection with heterologous viruses, similar to the wild-type infection.

A strategy based on TS-associated mutations and adjusted with tailor-made S proteins to target different variants

The identified TS substitutions were located in the viral nsps and did not affect the antigenicity of the S proteins. Thus, we hypothesized that we could design a vaccine platform against VOCs by exchanging the S protein of rTS-all with that of the other strains. To confirm this hypothesis, we constructed a recombinant virus (rTS-all-Omicron) containing the coding sequence of the Omicron S protein within the TS-all backbone (Figure 5A). As expected, rTS-all-Omicron exhibited a TS phenotype *in vitro* (Figure 5B). Furthermore, to evaluate its efficacy as a vaccine against Omicron, we measured the titer of neutralizing antibodies in the serum of hamsters 14 days after infection (Figure 5C). Consistent with our findings in Figure 4C, the titer against Omicron in the rTS-all-infected group was low (<32 at 14 dpi). However, infection with the rTS-all-Omicron significantly increased the titer of neutralizing antibodies against Omicron (128–256) but not that against the B-1 strain (<32), which has the D614G S protein (Figure 5D). These results confirmed that vaccination with rTS-all-Omicron is effective at protecting against Omicron, suggesting the possibility that rTS-all constitutes a powerful platform for the development of a COVID-19 live-attenuated vaccine by replacing the spike protein with that of newly emerging variants.

DISCUSSION

Live-attenuated viruses constitute a highly effective vaccine modality that has been used to treat various infectious diseases. They have several advantages including the induction of an effective humoral immune response and a long-lasting protective cellular immunity without the need for multiple doses. However, there are concerns regarding virulence reversion, such as that reported for oral poliovirus vaccines (Kew et al., 2005). In this study, we identified TS-associated mutations in several SARS-CoV-2 nsps that resulted in TS phenotypes of varying degrees of *in vitro* and *in vivo* attenuation in the Syrian hamster model (Figures 1 and S1B–S1D). To develop a safe and effective live-attenuated vaccine, we hypothesized that combining all these mutations may lead to a virus that is less likely to revert to the more pathogenic wild-type phenotype. Thus, we generated a recombinant virus, rTS-all, and confirmed that it retained TS characteristics *in vitro* and *in vivo*. More importantly, the generation of revertants proved to be less likely in comparison, both *in vitro* and *in vivo*, strengthening the potential use of rTS-all as a vaccine against COVID-19 (Figures 3 and S4).

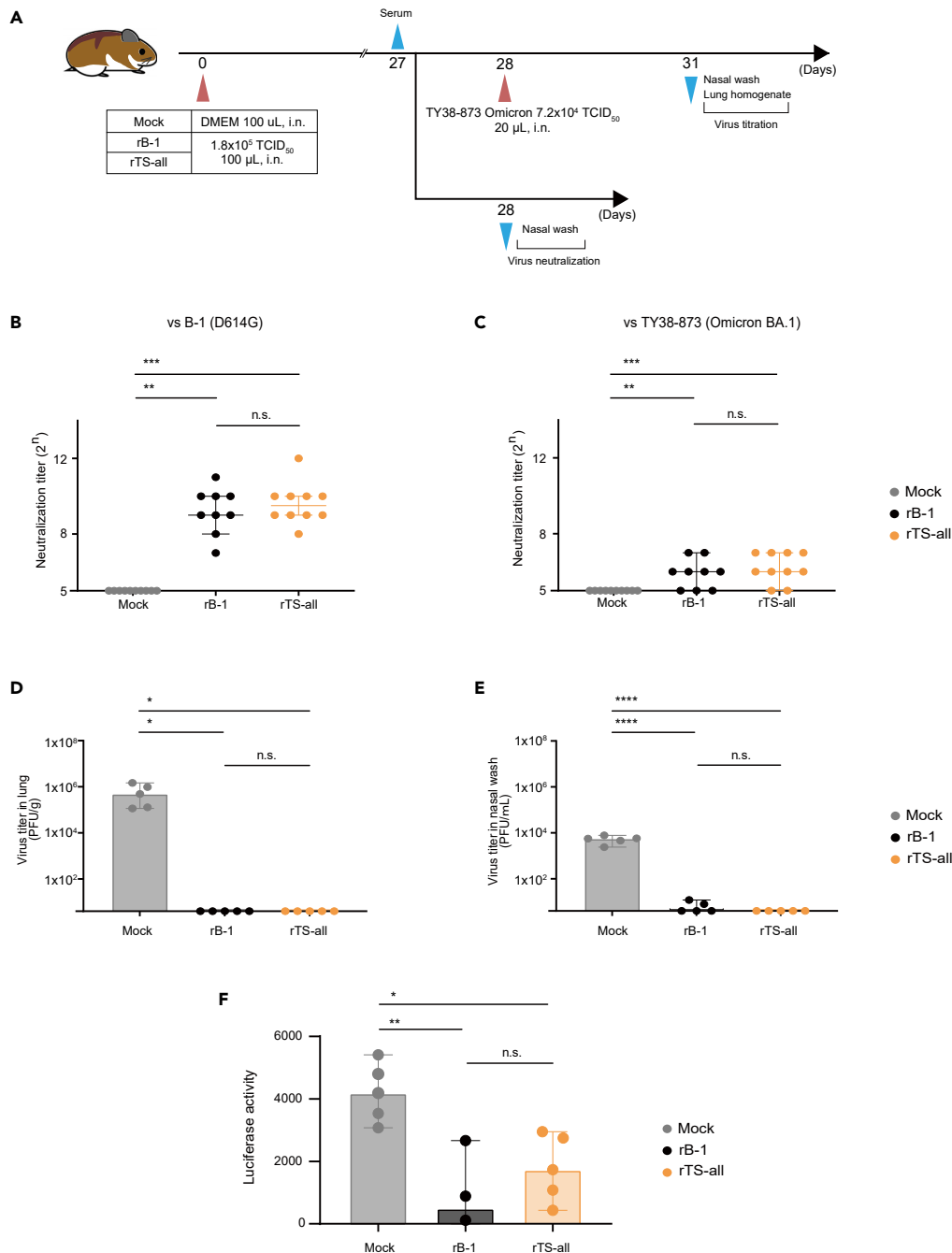


Figure 4. Live-attenuated TS viruses are effective against the variant Omicron

(A) Evaluation of the immunogenicity the rTS-all strain *in vivo*.

(B and C) Neutralization titers in the sera of immunized hamsters against the B-1 (B) and BA.1 viruses (C). Individual neutralization titers are plotted with symbols and bars showing the median values (Mock and rTS-all; $n = 10$, rB-1; $n = 9$). Error bars represent 95% CIs. The LOD is indicated in the x axis. Kruskal-Wallis test was used for statistical analysis (n.s.: not significant, ** $p < 0.01$ and *** $p < 0.001$).

(D and E) Viral titers in lung homogenates (D) and nasal wash specimens (E) three days post-infection. Viral titration was performed by plaque formation assays. Bars depict the mean values, and symbols represent individual viral titers ($n = 5$). Error bars represent mean SDs. The LOD is indicated in the x axis. For statistical analysis, one-way ANOVA was performed (n.s.: not significant, * $p < 0.05$, and **** $p < 0.0001$).

(F) Neutralization assay of the nasal wash specimens against pseudotyped VSV with D614G pre-alpha type spike. The symbols represent individual data and error bars represent SDs (Mock and rTS-all; $n = 5$, rB-1; $n = 3$). The data were statistically analyzed using one-way ANOVA (n.s.: not significant, * $p < 0.05$ and ** $p < 0.01$).

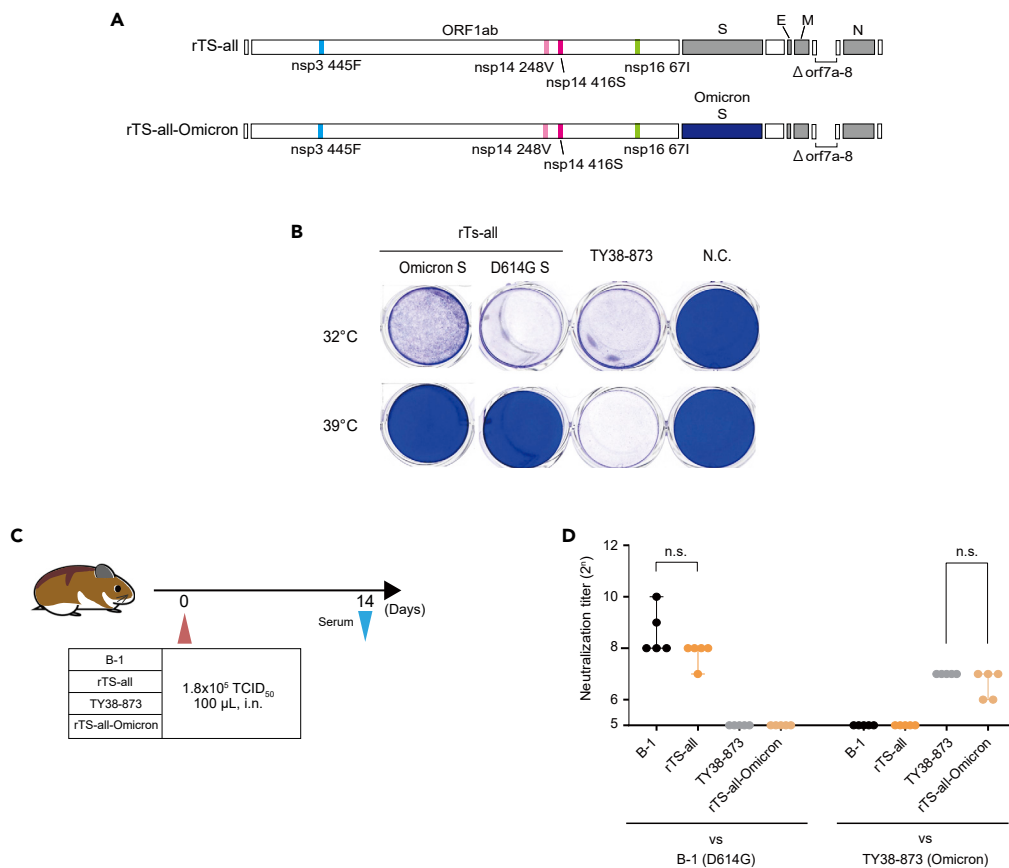


Figure 5. A strategy based on TS-associated mutations and adjusted with tailor-made S proteins to target different variants

(A) The construct of recombinant viruses which contained the Omicron spike with all the substitutions or deletions involved in temperature sensitivity.

(B) Temperature sensitivity of rTS-all-Omicron *in vitro*. VeroE6-TMPRSS II cells were infected with the recombinant strains and the Omicron variant and incubated under the indicated temperature conditions. CPE was observed three dpi by formalin fixation and crystal violet staining.

(C) Evaluation of the immunogenicity of the rTS-all-Omicron strain *in vivo* (n = 5).

(D) Neutralization titer of the sera from the hamsters infected with each strain. The individual neutralization titers are indicated with the corresponding symbols. Bars represent median values and error bars mean 95% CIs. For statistical analysis, the Kruskal-Wallis test was performed (n.s.: not significant). The LOD is indicated in the x axis.

One of the identified mutations resulted in a V67I substitution within the viral nsp16 protein, which is a 2-O-methyltransferase involved in viral genome replication (Chen et al., 2011; Decroly et al., 2008, 2011; Krafcikova et al., 2020). Structural analyses (AlphaFold2; Figure S2B) (Jumper et al., 2021) of this protein predicted no drastic differences compared with the wild-type version, consistent with the weak phenotype of the strain (H50-11). Another substitution was found in the MACS domain of nsp3 (L445F), accounting for the modest TS phenotypes of the L50-33 and L50-40 strains. In mouse hepatitis virus, mutations in the nsp3 MAC domain can cause temperature sensitivity, likely by enhancing proteasome-mediated degradation (Deng et al., 2019). Therefore, we speculated that the mechanisms underlying the TS phenotype in our isolated strains might be similar. Finally, several substitutions were identified in nsp14 (G248V, G416S, and A504V), rendering the resulting A50-18 strain more sensitive to higher temperatures. The predicted structure model suggested that both 248V and 416S substitutions affected hydrogen bonds (Figure S2A). The nsp14 protein has exo-ribonuclease and N7 methyltransferase domains and plays an important role in viral genome replication by forming a complex with other nsps (Chen et al., 2009; Min-skaia et al., 2006; Ogando et al., 2020). Therefore, at high temperatures, these structural changes may affect the molecular interactions within nsp14 itself and with other nsps, resulting in a decline in viral genome replication.

The strain, rTS-all, which combines all the above mutations, exhibited an attenuated phenotype while maintaining robust immunogenicity *in vivo* (Figure 3). Infection with rTS-all induced serum neutralizing antibodies against not only the homologous virus but also heterologous viruses, that were comparable to those induced by rB-1 infection (Figures 3H, 4B, and 4C). These results are most likely due to a more complex immunization process. Despite attenuation, the infecting virus stimulates several pathways of the immune system throughout its cycle within the infected cells (Shah et al., 2020), which might induce a highly effective immune response. A previous study has suggested that infection-induced primary memory B cells undergo more affinity maturation than vaccine-induced memory B cells do (Pape et al., 2021). Therefore, rTS-all infection may also induce mature B cells.

A previous study has reported that mucosal IgA against SARS-CoV-2 is present in convalescent patients and contributes to virus neutralization (Sterlin et al., 2021). However, it is not induced after vaccination with mRNA through the intramuscular route (Piano Mortari et al., 2021). An animal model study has reported that vaccination-induced systemic neutralizing antibodies failed to protect nasal tissue against SARS-CoV-2 infection (Zhou et al., 2021). Consistent with these studies, in the present study, we observed that intranasal administration of live-attenuated rTS-all induced neutralizing antibodies not only in the serum but also in the nasal mucosa, similar to the wild-type infection (Figures 4B, 4C, and 4F). Moreover, rTS-all-infected animals were protected from not only the B-1 strain but also the Omicron variant (Figures 3I, 4D, and 4E). We speculate that mucosal neutralizing antibodies induced by rTS-all intranasal administration might play an important role in protection against SARS-CoV-2 in peripheral areas.

A serious concern related to intranasal administration of live viruses is olfactory dysfunction, which has been reported after infection with SARS-CoV-2 (Giacomelli et al., 2020), probably as a consequence of nasal tissue damage (Khan et al., 2021; Urata et al., 2021). In this study, we confirmed that infection with A50-18 resulted in dramatically lower damage to the nasal tissue compared to infection with the wild-type strain. Therefore, our data suggest that the intranasal administration of rTS-all might constitute a safe option for the development of an effective vaccine strategy for protection against SARS-CoV-2 infections.

Previous studies have suggested that SARS-CoV-2 induces a broad, robust, and specific T cell response in convalescent individuals (Grifoni et al., 2020; Sekine et al., 2020). In our study, rTS-all exhibited a lower proliferation rate than the wild-type virus in the lungs, as well as less pathogenicity (Figure 3F). However, it replicated in the nasal cavity, which is a low-temperature region (Figure 3G). Although we did not assess cellular immunity in this study, infection with the rTS-all strain might elicit a T cell response similar to that of the wild-type strain.

Our study also offers a strong vaccine platform applicable to future variants. As nsp3, nsp14, and nsp16 do not affect the antigenicity of the S protein, alternative TS strains can be generated by changing the S coding sequence. Here, we confirmed that rTS-all-Omicron exhibited immunogenicity against the Omicron variant and conserved the TS phenotype characteristics of the original rTS-all strain.

Several live-attenuated vaccines have been reported in previous studies that were developed following different strategies. Ye et al. reported that a nsp16-deficient strain with a single point mutation (d16) was stable for 10 passages in Vero E6 cells (Ye et al., 2022). We have observed that the combination of several mutations renders rTS-all less prone to virulent reversion, both *in vitro* and *in vivo*, compared to single ones (Figure 3B and S4D). Therefore, we consider that rTS-all is a safer candidate for a live-attenuated vaccine. Another approach, cold-adaptation of virus was performed by Seo and Jang (Seo and Jang (2020)). This virus contained 11 unique amino acid substitutions, three of which were present in the spike protein, but the phenotype responsible mutations were not characterized in detail. Codon deoptimization of the spike coding sequence was attempted by Trimpert et al. and CODAGENIX (Trimpert et al., 2021; Wang et al., 2021). Compared with these strains, the advantage of the attenuated phenotype of the rTS-all strain lies in the amino acid substitutions outside of the spike protein, which is what varies the most among virus strains and which mainly shapes the protective immune response. Thus, it might constitute a suitable and versatile backbone where to insert spike proteins of emerging VOCs. Notably, we were able to generate the rTS-all-Omicron virus two weeks after the Omicron sequence was made available. Unlike the live-attenuated strains as mentioned above, the rTS-all strain has impaired replication at 37°C and conserves an immunogenicity comparable to the wild-type strain, based on its proliferation in the anterior regions of the nasal cavity, as was observed for the A50-18 strain (Figures 1G and 1H). Therefore, we believe that

rTS-all might be less likely to damage the olfactory epithelium. Moreover, from the production point of view, rTS-all shows normal replication at 32°C, which makes its amplification at manufacturing scales easily achievable, also reported by Seo and Jang, Trimpert et al., and Wang et al. Overall, our data suggest that this platform could be a promising candidate for the development of a live-attenuated vaccine that can be rapidly produced in response to new emerging variants or another SARS-CoV pandemic in the future.

Limitations of the study

Detailed characterization of the cellular and humoral immune responses was difficult using this model, due to the lack of hamster-specific reagents. Using a genetically modified mouse model could help circumvent this problem. Furthermore, it is unclear whether virulent reversion occurs during *in vivo* transmission, thus additional studies are required. In addition, olfactory functional analysis could help better determine its correlation with the nasal tissue injury, an important point for the development of intranasal attenuated vaccines.

STAR★METHODS

Detailed methods are provided in the online version of this paper and include the following:

- KEY RESOURCES TABLE
- RESOURCE AVAILABILITY
 - Lead contact
 - Materials availability
 - Data and code availability
- EXPERIMENTAL MODEL AND SUBJECT DETAILS
 - Ethical statement
 - Hamsters
 - Cell lines
 - Viruses
 - Evaluation of pathogenicity in hamsters
 - Evaluation of antigenicity in hamsters
- METHOD DETAILS
 - Plasmids
 - Construction of recombinant viruses using circular polymerase extension reaction (CPEr)
 - Titration assay
 - NGS analysis
 - *In vitro* and *in vivo* evaluation of the “reversion-to-virulence” risk of each mutant
- QUANTIFICATION AND STATISTICAL ANALYSIS

SUPPLEMENTAL INFORMATION

Supplemental information can be found online at <https://doi.org/10.1016/j.isci.2022.105412>.

ACKNOWLEDGMENTS

We appreciate the assistance from Mitsuyo Kosaka, Mai Matsumoto, and Manae Morishima (BIKEN). The authors acknowledge the NGS core facility of the Genome Information Research Center at the Research Institute for Microbial Diseases of Osaka University for their support with next-generation sequencing analyses. This work was supported by The Research Foundation for Microbial Diseases of Osaka University (BIKEN) and Japan Agency for Medical Research and Development (AMED) under Grant Number JP20pc0101047.

AUTHOR CONTRIBUTIONS

H.E. conceived and designed the study. A.Y. and S.O. conducted the majority of the experiments. S.T., C.O., and Y.M. constructed the CPER fragments for the construction of recombinant viruses. S.K. performed the pseudovirus neutralization assays. Hitomi S. performed the experiments related to the longitudinal evaluation of the immune response. Hidehiko S., S.U., and W.K. provided scientific insight. A.Y., S.O., and P.M. wrote the original manuscript and H.E. revised it. S.T., K.Y., and H.E. supervised the project.

DECLARATION OF INTERESTS

A.Y., S.O., S.K., Hitomi S., Hidehiko S., P.M., S.T., K.Y., and H.E. are employed by BIKEN. We report that A.Y., S.O., and H.E. are named on a patent that describes the use of the TS mutants as vaccines, currently being filed by BIKEN. Shiro T. and H.E. are managers of BIKEN. K.Y. is the director general of BIKEN.

Received: July 7, 2022

Revised: September 13, 2022

Accepted: October 18, 2022

Published: November 18, 2022

REFERENCES

- Baum, A., Fulton, B.O., Wloga, E., Copin, R., Pascal, K.E., Russo, V., Giordano, S., Lanza, K., Negron, N., Ni, M., et al. (2020). Antibody cocktail to SARS-CoV-2 spike protein prevents rapid mutational escape seen with individual antibodies. *Science* 369, 1014–1018. <https://doi.org/10.1126/science.abd0831>.
- Chen, Y., Cai, H., Pan, J., Xiang, N., Tien, P., Ahola, T., and Guo, D. (2009). Functional screen reveals SARS coronavirus nonstructural protein nsp14 as a novel cap N7 methyltransferase. *Proc. Natl. Acad. Sci. USA* 106, 3484–3489. <https://doi.org/10.1073/pnas.0808790106>.
- Chen, Y., Su, C., Ke, M., Jin, X., Xu, L., Zhang, Z., Wu, A., Sun, Y., Yang, Z., Tien, P., et al. (2011). Biochemical and structural insights into the mechanisms of SARS coronavirus RNA Ribose 2'-O-Methylation by nsp16/nsp10 protein complex. *PLoS Pathog.* 7, e1002294. <https://doi.org/10.1371/journal.ppat.1002294>.
- Cox, A., and Dewhurst, S. (2015). A single mutation at PB1 Residue 319 dramatically increases the safety of PR8 live attenuated influenza vaccine in a Murine model without compromising vaccine efficacy. *J. Virol.* 90, 2702–2705. <https://doi.org/10.1128/JVI.02723-15>.
- Decroly, E., Debarnot, C., Ferron, F., Bouvet, M., Coutard, B., Imbert, I., Gluais, L., Papageorgiou, N., Sharff, A., Bricogne, G., et al. (2011). Crystal structure and functional analysis of the SARS-coronavirus RNA cap 2'-O-methyltransferase nsp10/nsp16 complex. *PLoS Pathog.* 7, e1002059. <https://doi.org/10.1371/journal.ppat.1002059>.
- Decroly, E., Imbert, I., Coutard, B., Bouvet, M., Selisko, B., Alvarez, K., Gorbalenya, A.E., Snijder, E.J., and Canard, B. (2008). Coronavirus nonstructural protein 16 is a cap-0 binding enzyme possessing (nucleoside-2'-O)-methyltransferase activity. *J. Virol.* 82, 8071–8084. <https://doi.org/10.1128/JVI.00407-08>.
- Deng, X., Mettelman, R.C., O'Brien, A., Thompson, J.A., O'Brien, T.E., and Baker, S.C. (2019). Analysis of coronavirus temperature-sensitive mutants reveals an interplay between the Macrodome and papain-like protease impacting replication and pathogenesis. *J. Virol.* 93, e02140-18. <https://doi.org/10.1128/JVI.02140-18>.
- Edara, V.V., Norwood, C., Floyd, K., Lai, L., Davis-Gardner, M.E., Hudson, W.H., Mantus, G., Nyhoff, L.E., Adelman, M.W., Fineman, R., et al. (2021). Infection- and vaccine-induced antibody binding and neutralization of the B.1.351 SARS-CoV-2 variant. *Cell Host Microbe* 29, 516–521.e3. <https://doi.org/10.1016/j.chom.2021.03.009>.
- Folegatti, P.M., Ewer, K.J., Aley, P.K., Angus, B., Becker, S., Belij-Rammerstorfer, S., Bellamy, D., Bibi, S., Bittaye, M., Clutterbuck, E.A., et al. (2020). Safety and immunogenicity of the ChAdOx1 nCoV-19 vaccine against SARS-CoV-2: a preliminary report of a phase 1/2, single-blind, randomised controlled trial. *Lancet* 396, 467–478. [https://doi.org/10.1016/S0140-6736\(20\)31604-4](https://doi.org/10.1016/S0140-6736(20)31604-4).
- Giacomelli, A., Pezzati, L., Conti, F., Bernacchia, D., Siano, M., Oreni, L., Rusconi, S., Gervasoni, C., Ridolfo, A.L., Rizzardini, G., et al. (2020). Self-reported olfactory and taste disorders in patients with severe acute respiratory coronavirus 2 infection: a cross-sectional study. *Clin. Infect. Dis.* 71, 889–890. <https://doi.org/10.1093/cid/ciaa330>.
- Grifoni, A., Weiskopf, D., Ramirez, S.I., Mateus, J., Dan, J.M., Moderbacher, C.R., Rawlings, S.A., Sutherland, A., Premkumar, L., Jodi, R.S., et al. (2020). Targets of T Cell responses to SARS-CoV-2 coronavirus in humans with COVID-19 disease and unexposed individuals. *Cell* 181, 1489–1501.e15. <https://doi.org/10.1016/j.cell.2020.05.015>.
- Imai, M., Iwatsuki-Horimoto, K., Hatta, M., Loeber, S., Halfmann, P.J., Nakajima, N., Watanabe, T., Ujie, M., Takahashi, K., Ito, M., et al. (2020). Syrian hamsters as a small animal model for SARS-CoV-2 infection and countermeasure development. *Proc. Natl. Acad. Sci. USA* 117, 16587–16595. <https://doi.org/10.1073/pnas.2009799117>.
- Jackson, L.A., Anderson, E.J., Roupael, N.G., Roberts, P.C., Makhene, M., Coler, R.N., McCullough, M.P., Chappell, J.D., Denison, M.R., Stevens, L.J., et al. (2020). An mRNA vaccine against SARS-CoV-2 — preliminary report. *N. Engl. J. Med.* 383, 1920–1931. <https://doi.org/10.1056/NEJMoa2022483>.
- Jumper, J., Evans, R., Pritzel, A., Green, T., Figurnov, M., Ronneberger, O., Tunyasuvunakool, K., Bates, R., Židek, A., Potapenko, A., et al. (2021). Highly accurate protein structure prediction with AlphaFold. *Nature* 596, 583–589. <https://doi.org/10.1038/s41586-021-03819-2>.
- Kew, O.M., Sutter, R.W., de Gourville, E.M., Dowdle, W.R., and Pallansch, M.A. (2005). Vaccine-derived polioviruses and the endgame strategy for global polio eradication. *Annu. Rev. Microbiol.* 59, 587–635. <https://doi.org/10.1146/annurev.micro.58.030603.123625>.
- Khan, M., Yoo, S.-J., Clijsters, M., Backaert, W., Vanstapel, A., Speleman, K., Lietaer, C., Choi, S., Hether, T.D., Marcelis, L., et al. (2021). Visualizing in deceased COVID-19 patients how SARS-CoV-2 attacks the respiratory and olfactory mucosae but spares the olfactory bulb. *Cell* 184, 5932–5949.e15. <https://doi.org/10.1016/j.cell.2021.10.027>.
- Komase, K., Nakayama, T., Iijima, M., Milki, K., Kawanishi, R., and Uejima, H. (2006). The phosphoprotein of attenuated measles AIK-C vaccine strain contributes to its temperature-sensitive phenotype. *Vaccine* 24, 826–834. <https://doi.org/10.1016/j.vaccine.2005.06.036>.
- Krafcikova, P., Silhan, J., Nencka, R., and Boura, E. (2020). Structural analysis of the SARS-CoV-2 methyltransferase complex involved in RNA cap creation bound to sinefungin. *Nat. Commun.* 11, 3717. <https://doi.org/10.1038/s41467-020-17495-9>.
- Maassab, H.F., and Bryant, M.L. (1999). The development of live attenuated cold-adapted influenza virus vaccine for humans. *Rev. Med. Virol.* 9, 237–244. [https://doi.org/10.1002/\(sici\)1099-1654\(199910/12\)9:4<237::aid-rmv252>3.0.co;2-g](https://doi.org/10.1002/(sici)1099-1654(199910/12)9:4<237::aid-rmv252>3.0.co;2-g).
- Makino, S., Sasaki, K., Nazari, F., Nakagawa, M., and Nakamura, N. (1970). Cultivation of measles virus in sheep kidney cells. *Jpn. J. Microbiol.* 14, 501–504.
- Minskaia, E., Hertzog, T., Gorbalenya, A.E., Campanacci, V., Cambillau, C., Canard, B., and Ziebuhr, J. (2006). Discovery of an RNA virus 3' → 5' exoribonuclease that is critically involved in coronavirus RNA synthesis. *Proc. Natl. Acad. Sci. USA* 103, 5108–5113. <https://doi.org/10.1073/pnas.0508200103>.
- Murphy, B.R., and Coelingh, K. (2002). Principles underlying the development and use of live attenuated cold-adapted influenza A and B virus vaccines. *Viral Immunol.* 15, 295–323. <https://doi.org/10.1089/08822840260066242>.
- Ogando, N.S., Zevenhoven-Dobbe, J.C., van der Meer, Y., Bredenbeek, P.J., Posthuma, C.C., and Snijder, E.J. (2020). The enzymatic activity of the nsp14 exoribonuclease is critical for replication of MERS-CoV and SARS-CoV-2. *J. Virol.* 94, 012466-20. <https://doi.org/10.1128/JVI.01246-20>.
- Okamoto, K., Ami, Y., Suzuki, Y., Otsuki, N., Sakata, M., Takeda, M., and Mori, Y. (2016). Analysis of the temperature sensitivity of Japanese rubella vaccine strain TO-336.vac and its effect on immunogenicity in the guinea pig. *Virology* 491, 89–95. <https://doi.org/10.1016/j.virol.2016.01.027>.
- Pape, K.A., Dileepan, T., Kabage, A.J., Kozysa, D., Batres, R., Evert, C., Matson, M., Lopez, S.,

- Krueger, P.D., Graiziger, C., et al. (2021). High-affinity memory B cells induced by SARS-CoV-2 infection produce more plasmablasts and atypical memory B cells than those primed by mRNA vaccines. *Cell Rep.* 37, 109823. <https://doi.org/10.1016/j.celrep.2021.109823>.
- Parks, C.L., Lerch, R.A., Walpita, P., Wang, H.P., Sidhu, M.S., and Udem, S.A. (2001). Comparison of predicted amino acid sequences of measles virus strains in the Edmonston vaccine lineage. *J. Virol.* 75, 910–920. <https://doi.org/10.1128/JVI.75.2.910-920.2001>.
- Piano Mortari, E., Russo, C., Vinci, M.R., Terreri, S., Fernandez Salinas, A., Piccioni, L., Alteri, C., Colagrossi, L., Coltella, L., Ranno, S., et al. (2021). Highly specific memory B cells generation after the 2nd dose of BNT162b2 vaccine compensate for the decline of serum antibodies and absence of mucosal IgA. *Cells* 10, 2541.
- Sahin, U., Muik, A., Derhovanessian, E., Vogler, I., Kranz, L.M., Vormehr, M., Baum, A., Pascal, K., Quandt, J., Maurus, D., et al. (2021). Publisher correction: COVID-19 vaccine BNT162b1 elicits human antibody and TH1 T cell responses. *Nature* 590, E17. <https://doi.org/10.1038/s41586-020-03102-w>.
- Sasaki, K. (1974). Studies on the modification of the live AIK measles vaccine. I. adaptation of the further attenuated AIK measles virus (the strain AIK-L33) to chick embryo cells. *Kitasato Arch. Exp. Med.* 47, 1–12.
- Sekine, T., Perez-Potti, A., Rivera-Ballesteros, O., Strålin, K., Gorin, J.-B., Olsson, A., Llewellyn-Lacey, S., Kamal, H., Bogdanovic, G., Muschiol, S., et al. (2020). Robust T cell immunity in convalescent individuals with asymptomatic or mild COVID-19. *Cell* 183, 158–168.e14. <https://doi.org/10.1016/j.cell.2020.08.017>.
- Seo, S.H., and Jang, Y. (2020). Cold-adapted live attenuated SARS-CoV-2 vaccine completely protects human ACE2 transgenic Mice from SARS-CoV-2 infection. *Vaccines (Basel)* 8, 584. <https://doi.org/10.3390/vaccines8040584>.
- Shah, V.K., Fimal, P., Alam, A., Ganguly, D., and Chattopadhyay, S. (2020). Overview of immune response during SARS-CoV-2 infection: lessons from the past. *Front. Immunol.* 11, 1949. <https://doi.org/10.3389/fimmu.2020.01949>.
- Shishido, A., and Ohtawara, M. (1976). Development of attenuated rubella virus vaccines in Japan. *Jpn. J. Med. Sci. Biol.* 29, 227–253. <https://doi.org/10.7883/yoken1952.29.227>.
- Sia, S.F., Yan, L.M., Chin, A.W.H., Fung, K., Choy, K.T., Wong, A.Y.L., Kaewpreedee, P., Perera, R.A.P.M., Poon, L.L.M., Nicholls, J.M., et al. (2020). Pathogenesis and transmission of SARS-CoV-2 in golden hamsters. *Nature* 583, 834–838. <https://doi.org/10.1038/s41586-020-2342-5>.
- Sterlin, D., Mathian, A., Miyara, M., Mohr, A., Anna, F., Claër, L., Quentric, P., Fadlallah, J., Devilliers, H., Ghillani, P., et al. (2021). IgA dominates the early neutralizing antibody response to SARS-CoV-2. *Sci. Transl. Med.* 13, eabd2223. <https://doi.org/10.1126/scitranslmed.abd2223>.
- Takahashi, M., Otsuka, T., Okuno, Y., Asano, Y., and Yazaki, T. (1974). Live vaccine used to prevent the spread of varicella in children in hospital. *Lancet* 2, 1288–1290. [https://doi.org/10.1016/s0140-6736\(74\)90144-5](https://doi.org/10.1016/s0140-6736(74)90144-5).
- Tani, H., Shiokawa, M., Kaname, Y., Kambara, H., Mori, Y., Abe, T., Moriishi, K., and Matsuura, Y. (2010). Involvement of ceramide in the propagation of Japanese encephalitis virus. *J. Virol.* 84, 2798–2807. <https://doi.org/10.1128/JVI.02499-09>.
- Torii, S., Ono, C., Suzuki, R., Morioka, Y., Anzai, I., Fauzyah, Y., Maeda, Y., Kamitani, W., Fukuhara, T., and Matsuura, Y. (2021). Establishment of a reverse genetics system for SARS-CoV-2 using circular polymerase extension reaction. *Cell Rep.* 35, 109014. <https://doi.org/10.1016/j.celrep.2021.109014>.
- Trimpert, J., Dietert, K., Firsching, T.C., Ebert, N., Thi Nhu Thao, T., Vladimirova, D., Kaufer, S., Labrousse, F., Abdelgawad, A., Conradie, A., et al. (2021). Development of safe and highly protective live-attenuated SARS-CoV-2 vaccine candidates by genome recoding. *Cell Rep.* 36, 109493. <https://doi.org/10.1016/j.celrep.2021.109493>.
- Urata, S., Maruyama, J., Kishimoto-Urata, M., Sattler, R.A., Cook, R., Lin, N., Yamasoba, T., Makishima, T., and Paessler, S. (2021). Regeneration profiles of olfactory epithelium after SARS-CoV-2 infection in golden Syrian hamsters. *ACS Chem. Neurosci.* 12, 589–595. <https://doi.org/10.1021/acscchemneuro.0c00649>.
- Wang, Y., Yang, C., Song, Y., Coleman, J.R., Stawowczyk, M., Tafrova, J., Tasker, S., Boltz, D., Baker, R., Garcia, L., et al. (2021). Scalable live-attenuated SARS-CoV-2 vaccine candidate demonstrates preclinical safety and efficacy. *Proc. Natl. Acad. Sci. USA* 118, e2102775118. <https://doi.org/10.1073/pnas.2102775118>.
- Wibmer, C.K., Ayres, F., Hermanus, T., Madzivhandila, M., Kgagudi, P., Oosthuysen, B., Lambson, B.E., de Oliveira, T., Vermeulen, M., van der Berg, K., et al. (2021). SARS-CoV-2 501Y.V2 escapes neutralization by South African COVID-19 donor plasma. *Nat. Med.* 27, 622–625. <https://doi.org/10.1038/s41591-021-01285-x>.
- Ye, Z.W., Ong, C.P., Tang, K., Fan, Y., Luo, C., Zhou, R., Luo, P., Cheng, Y., Gray, V.S., Wang, P., et al. (2022). Intranasal administration of a single dose of a candidate live attenuated vaccine derived from an NSP16-deficient SARS-CoV-2 strain confers sterilizing immunity in animals. *Cell. Mol. Immunol.* 19, 588–601. <https://doi.org/10.1038/s41423-022-00855-4>.
- Zhou, D., Chan, J.F.-W., Zhou, B., Zhou, R., Li, S., Shan, S., Liu, L., Zhang, A.J., Chen, S.J., Chan, C.C.-S., et al. (2021). Robust SARS-CoV-2 infection in nasal turbinates after treatment with systemic neutralizing antibodies. *Cell Host Microbe* 29, 551–563.e5. <https://doi.org/10.1016/j.chom.2021.02.019>.
- Zimmerman, L.A., Reef, S.E., and Orenstein, W.A. (2018). Rubella vaccine-A tale of appropriate caution and remarkable success. *JAMA Pediatr.* 172, 95–96. <https://doi.org/10.1001/jamapediatrics.2017.4178>.

STAR★METHODS

KEY RESOURCES TABLE

REAGENT or RESOURCE	SOURCE	IDENTIFIER
Bacterial and virus strains		
SARS-CoV-2: pre-alpha type, D614G, B-1 strain	This paper	NCBI: LC603286
SARS-CoV-2: gamma variant, TY7-501 strain	National Institute of Infectious Diseases	GISAID ID : EPI_ISL_833366
SARS-CoV-2: delta variant, BK325 strain	Research Foundation for Microbial Diseases of Osaka University	N/A
SARS-CoV-2: omicron variant, TY38-873 strain	National Institute of Infectious Diseases	GISAID ID : EPI_ISL_7418017
Chemicals, peptides, and recombinant proteins		
5-fluorouracil	FUJIFILM Wako	Cat# 068-01401
KOD One PCR Master Mix -Blue-	TOYOBO	Cat# KMM-201
PrimeSTAR GXL DNA polymerase	TaKaRa Bio	Cat# R050A
Lipofectamin LTX Reagent with PLUS™ Reagent	Invitrogen	Cat# 15338100
SeaPlaque Agarose	LONZA	Cat# 50100
TriReagent	Molecular Research Center	Cat# TR118
Luciferase Cell Culture Lysis 5X Reagent	Promega	Cat# E153A
Hematoxylin	Sakura Finetek Japan	Cat# 9130-4P
1% Eosin Y Solution	FUJIFILM Wako	Cat# 051-06515
Critical commercial assays		
QIAamp viral RNA mini kit	Qiagen	Cat# 52904
Luciferase Assay System	Promega	Cat# E8130
SuperScript™ III First-Strand Synthesis System for RT-PCR	Invitrogen	Cat# 11904018
ONE-Glo™ EX Luciferase Assay System	Promega	Cat# E8110
DNA Ligation Kit Ver.2.1	TaKaRa Bio	Cat# 6022
Deposited data		
Viral genome sequence of B-1 strain	This paper	NCBI: LC603286
Viral genome sequence of A50-18 strain	This paper	NCBI: LC603287
Viral genome sequence of H50-11 strain	This paper	NCBI: LC603288
Viral genome sequence of L50-33 strain	This paper	NCBI: LC603289
Viral genome sequence of L50-40 strain	This paper	NCBI: LC603290
Experimental models: Cell lines		
Human: 293T cells	ATCC	Cat# CRL-3216; PRID: CVCL_0063
Green monkey: Vero cells	ATCC	Cat# CCL-81; RRID: CVCL_0059
Green monkey: Vero cells with constitutive expression of TMPRSS II, VeroE6-TMPRSS II cells	Japanese Collection of Research Bioresources Cell Bank	Cat# JCRB1819; RRID: CVCL_YQ49
Syrian hamster: BHK-21(C-13) cells	Japanese Collection of Research Bioresources Cell Bank	Cat# JCRB9020; RRID: CVCL_1915
Syrian hamster: BHK-21(C-13) cells with constitutive expression of hACE2, BHK-hACE2 cells	This paper	N/A

(Continued on next page)

Continued

REAGENT or RESOURCE	SOURCE	IDENTIFIER
<i>Experimental models: Organisms/strains</i>		
Syrian hamster (male, 5 weeks old)	SLC	Slc:Syrian
<i>Oligonucleotides</i>		
CoV-2-F1-Fw (CTATATAAGCAGA GCTCGTTTAGTGA ACCGTattaaggtttatacctcccaggtaac)	Torii et al. (2021)	N/A
CoV-2-F1-Rv (cagattcaactgcatggcatt gttagtagccttattaaggctcctgc)	Torii et al. (2021)	N/A
CoV-2-F2-Fw (gcaggagccttaataagg ctactaacaatgccatgcaagttgaatctg)	Torii et al. (2021)	N/A
CoV-2-F2-Rv (ggtaggattttccactactt cttcagagactggttttagatcttcgacggc)	Torii et al. (2021)	N/A
CoV-2-F3-Fw (gcctgcgaagatctaaacca gtctctgaagaagtagtggaatacctacc)	Torii et al. (2021)	N/A
CoV-2-F3-Rv (gggtcacagcgcagcttc ttcaaaagtactaaagg)	Torii et al. (2021)	N/A
CoV-2-F4-Fw (caccactaattcaactattg gtgctttggacatcagcatctatagtagctgtggtg)	Torii et al. (2021)	N/A
CoV-2-F4-Rv (gtttaaaacgattgtgcatca gtgactg)	Torii et al. (2021)	N/A
CoV-2-F5-Fw (cacagtctgtaccgtctgcggtatg tggaagggttatggctgtagtgtgatc)	Torii et al. (2021)	N/A
CoV-2-F5-Rv (gcggtgtgtacatagcctcata aaactcaggttccaatacttgaagtg)	Torii et al. (2021)	N/A
CoV-2-F6-Fw (cactcaagggtattgggaacctga gtttatgaggctatgtacacaccgc)	Torii et al. (2021)	N/A
CoV-2-F6-Rv (catacaaaactgccaccatcacacca ggcaaggttaaggttagatagcactctag)	Torii et al. (2021)	N/A
CoV-2-F7-Fw (ctagagtgtctatcaaccttaa cttgctgtgtgtgatgggtgcagttgtatg)	Torii et al. (2021)	N/A
CoV-2-F7-Rv (ctagagactagtggaataaaa acaagaaaaacaacattgttcgttagttgtaac)	Torii et al. (2021)	N/A
CoV-2-F8-Fw (gttaacaactaaacgaa caatgtttgtttctgtttattgccactagtctctag)	Torii et al. (2021)	N/A
CoV-2-F8-Rv (gcagcaggatccacaaga acaacagcccttgagacaactacagcaactgg)	Torii et al. (2021)	N/A
CoV-2-F9-Fw (ccagttgctgtagtgtctcaa gggctgtgttctgttgatcctgctgc)	Torii et al. (2021)	N/A
CoV-2-F9-Rv (caatctcattggtgtctctcatc)	Torii et al. (2021)	N/A
CoV-2-F10-Fw (gatgaagagcaaccaatggagattg)	Torii et al. (2021)	N/A
CoV-2-F10-Rv (GGAGATGCCATGCCGACC Cttttttttttttttttttttgtcattctcctaag)	Torii et al. (2021)	N/A
CoV-2-Linker-Fw (cttaggagaatgacaaaaaaaaaaaaa aaaaaaaaaaaaGGGTGCGCATGGCATCTCC)	Torii et al. (2021)	N/A
CoV-2-Linker-Rv (gttacctgggaa ggataaacctttaatACGGTTCACTAAACGAG CTCTGCTTATATAG)	Torii et al. (2021)	N/A

(Continued on next page)

Continued

REAGENT or RESOURCE	SOURCE	IDENTIFIER
CoV-2-TS-F6-Rv (catacaaactgccactatcaca accaggcaagttaaggtagatagcactctag)	This paper	N/A
CoV-2-TS-F7-Fw (ctagagtgtctatcaaccttaa ctgctggtgtgtagatggcagttgtatg)	This paper	N/A
CoV-2-4052T-Fw (tatattgacattaatggc aatttcatccagattctgcca)	This paper	N/A
CoV-2-4052T-Rv (ttgccattaatgcaataaa agtaacaagtttctgtga)	This paper	N/A
CoV-2-18782T-Fw (tgattgatgttcaacaatg ggttttacaggtaacctaca)	This paper	N/A
CoV-2-18782T-Rv (ccattgtgaacatcaatc ataaacggattatagacgtaa)	This paper	N/A
CoV-2-19285A-Fw (aaccttaactgcctgg ttgtgatgtggcagttgtatg)	This paper	N/A
CoV-2-19285A-Rv (caaccaggcaagtta aggttagatagcactctagtgtcaa)	This paper	N/A
CoV-2-19550T-Fw (tctcgtgcttataacatga tgatctcagttggcttagc)	This paper	N/A
CoV-2-19550T-Rv (tcattgtataagcatcgaga tacaatctgtactcattagc)	This paper	N/A
CoV-2-20857A-Fw (ctgtaccctataatagaga attatacattttggtgctgttct)	This paper	N/A
CoV-2-20857A-Rv (tctcatattatagggtacag ctaatgttaattgtttaaa)	This paper	N/A
CoV-2-G2-Fw (cggcagtgaggacaatcag acaactac)	Torii et al. (2021)	N/A
CoV-2-G2-Rv (ggccttagcataattagctata gtatccaaggagac)	Torii et al. (2021)	N/A
CoV-2-G6-Fw (tgtatgatatacgtaaa aacagatggtacac)	Torii et al. (2021)	N/A
CoV-2-G6-Rv (aacgtgttatacacgtagcag actttagtgtac)	Torii et al. (2021)	N/A
CoV-2-G7-Fw (aaaggttcaacacatg gttgttaaagctgc)	Torii et al. (2021)	N/A
CoV-2-G7-Rv (cgtacatttg ttctgagagagggc)	Torii et al. (2021)	N/A
covid-dp-4655-4683r (ggcactttgaga gatctcatataccgagc)	Torii et al. (2021)	N/A
covid-dp-18160-18186f (gttgacata cctggcatacctaaggac)	Torii et al. (2021)	N/A
covid-dp-19712-19738r (caacaccatca acttttgtaaacag)	Torii et al. (2021)	N/A
covid-dp-20470-20496f (gcgcaaacaggtt catctaagtgtgtg)	Torii et al. (2021)	N/A
Recombinant DNA		
PB-CMV-MCS-EF1-RedPuro	Systembiosciences	Cat# PB514B-2
pCSII-sars-cov-2 F1+2	This paper	N/A
pCSII-sars-cov-2 F3	This paper	N/A

(Continued on next page)

Continued

REAGENT or RESOURCE	SOURCE	IDENTIFIER
pCSII-sars-cov-2 F4	This paper	N/A
pCSII-sars-cov-2 F5	This paper	N/A
pcDNA3.1.-sars-cov2 F6	This paper	N/A
pcDNA3.1.-sars-cov2 F7	This paper	N/A
pCSII-sars-cov-2 F8	This paper	N/A
pCSII-sars-cov-2 F9	This paper	N/A
pCSII-sars-cov-2 F10+11+12	This paper	N/A
Software and algorithms		
PRISM	GraphPad Software	Version 7.02
Pymol	Schrodinger	https://www.pymol.org/
Alphafold2	Jumper et al. (2021)	N/A

RESOURCE AVAILABILITY

Lead contact

Further requests for resources and reagents should be directed to and will be fulfilled by the lead contact, Hirotaka Ebina (hebina@biken.osaka-u.ac.jp).

Materials availability

The principal authors of this paper are employees of the Research Foundation for Microbial Diseases of Osaka University (BIKEN). Therefore, the distribution of the TS strains and their composite strains obtained in this study requires the establishment of an MTA with BIKEN.

Data and code availability

The data in this report are available from the [lead contact](#) upon request. The viral genome sequences of the TS mutants isolated in this study have been deposited at the National Center for Biotechnology Information (Accession numbers 5 for B-1, A50-18, H50-11, L50-33 and L50-40 are LC603286, LC603287, LC603288, LC603289 and LC603290, respectively). All other data needed to evaluate the conclusions in the paper are present in the paper or the [supplemental information](#). Additional information for reanalysis is shared by the [lead contact](#) upon request.

EXPERIMENTAL MODEL AND SUBJECT DETAILS

Ethical statement

All animal experimental protocols, including anesthesia conditions, endpoints for infection, and euthanasia methods; and genetic recombination experiments, were reviewed and approved by the corresponding Osaka University's Review Committees (approval no. R02-10, approval no. 4680, respectively).

Hamsters

Male Syrian hamsters (SLC:Syrian, 4-weeks old) were purchased from Japan SLC, Inc (Shizuoka, Japan). Hamsters were housed under a 12-h light/12-h dark cycle and were allowed free access to food and water. Hamsters were used for each experiment after a 1-week adjustment period.

Cell lines

Vero cells (African green monkey kidney cells: ATCC, CCL-81) and 293T cells (human embryonic kidney cells: ATCC, CRL-3216) were maintained at 37°C in Dulbecco's modified Eagle's Medium (DMEM, Sigma-Aldrich, Cat# D6429) supplemented with 10% heat-inactivated fetal bovine serum (FBS, Sigma-Aldrich), penicillin (100 U/mL), and streptomycin (0.1 mg/mL) (PS, Gibco, Cat# 1154887). VeroE6-TMPRSS2 cells (TMPRSS2-expressing Vero cells: JCRB, JCRB1819) were maintained at 37°C in DMEM supplemented with 10% heat-inactivated FBS, PS, and 1 mg/mL G418 Sulfate (Gibco, Cat# 10131027). BHK cells (hamster kidney cells: JCRB, JCRB9020) were maintained at 37°C in Minimum Essential Medium Eagle (MEM, Sigma-Aldrich, Cat# M4655) supplemented with 10% heat-inactivated FBS and PS. BHK cells

stably expressing human ACE2 were generated by piggyBac plasmid transfection and puromycin-based selection and maintained with 3 µg/mL puromycin (Gibco, Cat# A1113803).

Viruses

SARS-CoV-2 was isolated from a SARS-CoV-2-positive clinical specimen in Osaka City, Japan. An aliquot of 500 µL of the specimen was diluted with 500 µL of Dulbecco's phosphate-buffered saline (D-PBS, Nacalai Tesque, Cat# 14249) and filtered through a 0.22 µm filter. One hundred microliters of this filtrate were used to inoculate the Vero cells. Cytopathic effects (CPE) were observed three days post-infection (dpi). The supernatant was collected and stored at −80°C as the "SARS-CoV-2 clinical isolate strain B-1". Whole-genome sequencing of B-1 was performed using next-generation sequencing (NGS) analysis, as described below. The sequencing results showed that the B-1 strain had a D614G substitution in the S protein. The SARS-CoV-2 delta variant (BK325) was provided by the Research Foundation for Microbial Diseases of Osaka University. The gamma (hCoV-19/Japan/TY7-501/2021, GISAID ID: EPI_ISL_833366) and Omicron variants (TY38-873, GISAID ID: EPI_ISL_7418017) were obtained from the National Institute of Infectious Diseases of Japan (NIID).

A pseudotyped vesicular stomatitis virus (VSV) with the SARS-CoV-2 S protein (pre-alpha type: D614G) was constructed for neutralization assays. The pCAGGS plasmid encoding the codon-optimized SARS-CoV-2 spike gene lacking the C-terminal 19 amino acids was transfected into 293T cells using polyethylenimine (Polysciences, Cat# 24765). Twenty-four hours post-transfection, VSVΔG/Luc-complemented VSV G pseudovirus, where the VSV G gene was replaced by the luciferase gene but expressed VSV G on the surface of the virion (VSVΔG/Luc complemented with VSV G), was used to infect cells at multiplicity of infection (MOI) = 0.1 (Tani et al., 2010). The excess unattached virus was eliminated by removing the supernatant two hours post-infection and replacing it with a fresh medium. After 72 h of incubation at 37°C, the cell culture supernatants containing VSVΔG/Luc-encoding SARS-CoV-2 S-expressing pseudovirus were collected and filtered through a 0.45 µm pore size filter.

Evaluation of pathogenicity in hamsters

Syrian hamsters (Slc:Syrian) were purchased from Japan SLC, Inc. Five-week-old male hamsters were anesthetized with 2.0-3.0% isoflurane (FUJIFILM Wako, Cat# 1349003) inhalation and 0.3 mg/kg medetomidine (Nippon Zenyaku Kogyo) + 4 mg/kg midazolam (Maruishi Pharmaceutica) + 5 mg/kg butorphanol (Meiji Seika Pharma) intraperitoneal injection. One hundred microliters of DMEM containing the respective SARS-CoV-2 strains were delivered dropwise to the nostrils, and body weight was measured daily. For the assessment of acute symptoms, lung and nasal wash specimens were collected with 1 mL of D-PBS at three dpi. The lungs were divided into left and four right lungs. The left lung was fixed with 10% formalin and serially sectioned. One section was stained with hematoxylin (Sakura Finetek Japan, Cat# 9130-4P) and eosin (FUJIFILM Wako, Cat# 051-06515). The right lung was homogenized with Biomasher II (Nippi, Cat# 320 103) and suspended in 1 mL of DMEM. After centrifugation at 100 g for 5 min, the supernatant was collected as lung homogenate. The viral titers of these samples were evaluated using a plaque formation assay. To evaluate the tissue damage in the nasal cavity caused by infection with the TS mutants, hamsters were infected with SARS-CoV-2 B-1 or A50-18 strains contained in 20 µL of DMEM via the intranasal route to limit the administration to the upper respiratory tract. After euthanasia, the heads were fixed in 10% formalin and sectioned. Each section was stained with hematoxylin and eosin (HE).

Evaluation of antigenicity in hamsters

To analyze antigenicity, we performed a re-challenge assay and evaluated the presence of neutralizing antibodies in the serum and nasal wash specimens. Hamsters who recovered from the SARS-CoV-2 primary infection were re-challenged with DMEM containing the respective SARS-CoV-2 strains three weeks after the first infection. Body weight changes were recorded for an additional 8-10 d. For the neutralization assay, blood and nasal wash specimens were collected from the recovered hamsters. The blood specimens were centrifuged at 800 g for 10 min, and serum was collected for analysis. Nasal wash specimens were filter-sterilized prior to the assay.

METHOD DETAILS

Plasmids

The hACE2 gene was cloned into the piggyBac plasmid (Systembiosciences, PB514B-2). Briefly, total RNA was extracted from 293T cells and reverse-transcribed using the SuperScript™ III First-Strand Synthesis System for RT-PCR (Invitrogen, Cat# 11904018). Then, hACE2 complementary DNA (cDNA) was amplified

using the KOD One PCR Master Mix -Blue- (TOYOBO, Cat# KMM-201). The obtained fragment was digested with XbaI (NEB, Cat# R0145) and NotI (NEB, Cat# R0189) and ligated with PB514B-2, which was also digested with XbaI and NotI, using the TAKARA Ligation kit ver.2.1 (TAKARA Bio, Cat# 6022).

Isolation of TS mutants

To obtain TS mutants, a previously reported protocol for the induction of mutations in MHV was followed (Deng et al., 2019). Briefly, the clinical isolate strain B-1 was used to infect confluent Vero cells in six-well plates for 1 h at 37°C. A fresh medium containing 5-fluorouracil (100 µg/mL, FUJIFILM Wako, Cat# 068-01401) was added. After a one-day incubation period at 32°C, the supernatants were collected and stocked as “mutated virus”. These viruses were passaged three times in Vero cells at 32°C, and viral clones were obtained by plaque isolation. The collected plaques were suspended in 100 µL DMEM and an aliquot of 2–50 µL of this suspension was used to infect Vero cells at 32°C. To confirm temperature sensitivity, we observed the development of CPE at 37 or 32°C.

Construction of recombinant viruses using circular polymerase extension reaction (CPE)

Viruses bearing TS mutations were constructed using circular polymerase extension reaction (CPE) (Torii et al., 2021), with minor modifications. We cloned the fragmented B-1 viral genome into plasmids. TS mutations of interest were introduced into these plasmids using inverse PCR. We then assembled these fragments by CPE using PrimeSTAR GXL DNA polymerase (Takara Bio, Cat# R050A). The assembled cDNA was transfected into BHK-hACE2 cells using Lipofectamine LTX Reagent with PLUS™ Reagent (Invitrogen, Cat# 15338100). Seven days after transfection, supernatants were collected. The supernatant was used to inoculate VeroE6-TMPRSS2 and incubated for four days. After observing CPE, the supernatant was collected and used to inoculate Vero cells to harvest the desired SARS-CoV2 viruses. To obtain TS-recombinant viruses, we performed a construction experiment at 32–34°C.

Titration assay

Viral titration was determined using the 50% tissue culture infectious dose (TCID₅₀) or plaque formation units (PFU). Briefly, samples were serially diluted in DMEM supplemented with 2% FBS and antibiotics. Fifty microliters of diluted samples were used to infect confluent Vero cells in 96-well plates and incubated at 37°C (wild-type strain) or 32°C (TS strain) for six days. Infected cells were fixed with 10% formalin and stained with crystal violet. After staining, the TCID₅₀ was calculated using the Behrens-Karber method. For the plaque formation assay, diluted samples were used to infect confluent Vero cells in 6-well plates for 1 h at 32 or 37°C. Cells were then washed with D-PBS. After washing, a fresh medium containing 1% SeaPlaque Agarose (Lonza, Cat# 50100) was layered and incubated at 32 or 37°C until plaque formation. Cells were fixed in 10% formalin and stained with crystal violet. Visible plaques were counted to calculate the PFU.

NGS analysis

Vero cells were infected with wild-type or TS SARS-CoV-2 and incubated at 37 or 32°C, respectively. After three days, supernatants were collected, and RNA was extracted using a QIAamp Viral RNA Mini Kit (Qia-gen, Cat# 52904) according to the manufacturer’s protocol. Viral RNA was processed and analyzed at the Genome Information Research Center of Osaka University using NovaSeq6000 (Illumina). Wuhan strain (NC045512) was used as the reference sequence.

Determination of viral growth dynamics

One million Vero cells per well were cultured in six-well plates and incubated at 37°C overnight. SARS-CoV-2 strain suspensions (1×10^4 TCID₅₀) were used to inoculate the cells (MOI = 0.01), which were then incubated at 32, 34, 37, or 39°C for five days. The supernatants were collected and stored at –80°C daily. Viral titration of the supernatants was performed using TCID₅₀/mL, as described above. Each experiment was performed in triplicate.

Neutralization assay

Serum samples were inactivated by incubation at 56°C for 30 min and serially diluted with DMEM supplemented with 2% FBS. Serially diluted serum was mixed with 100 TCID₅₀ of SARS-CoV-2 B-1, Delta, Gamma, or Omicron strains and incubated at 37°C for 1 h. After incubation, the samples were used to inoculate confluent Vero cells in 96-well plates and were incubated at 37°C for seven days. Cells were fixed in formalin

and stained with crystal violet. Neutralizing titers were determined as the inverse of the maximum dilution that prevented viral proliferation.

For the neutralization assay of nasal wash specimens, we performed an assay using the pseudotyped VSV virus. Briefly, the VSVΔG/Luc-encoding SARS-CoV-2 S-expressing pseudovirus was mixed and co-incubated with the same volume of nasal wash and incubated for one hour. Mixtures were added to Vero cells and the cells were lysed using lysis buffer (Promega, Cat# E153A) after incubation for 24 h. Luciferase activity was measured using a ONE-Glo™ EX Luciferase Assay System (Promega, Cat# E8130).

Generation and characterization of revertants

To obtain revertants, TS strains were used to infect confluent Vero cells at 37, 38, and 39°C (MOI = 1). Viruses from the CPE-positive wells were further propagated in Vero cells at 37 or 38°C to obtain the corresponding viral stocks. To identify any mutations around the nucleotide of interest in the revertants, viral genomic RNA was extracted using TriReagent (Molecular Research Center, Cat# TR118) or a QIAamp viral RNA mini kit (Qiagen, Cat# 52904), according to the manufacturer's protocols, and subsequently subjected to cDNA synthesis using the SuperScript™ III First-Strand Synthesis System for RT-PCR (Invitrogen, Cat# 11904018). The genomic regions surrounding each mutation of interest in Table 1 were amplified by PCR using specific primers. The PCR products were sequenced and compared with those of the corresponding parental TS strains.

In vitro and in vivo evaluation of the "reversion-to-virulence" risk of each mutant

To estimate the risk of each TS strain reverting to the virulent phenotype *in vitro*, each TS virus was used to infect confluent Vero cells (5×10^3 TCID₅₀/well) in 96-well plates, which were maintained for one or two days at 32°C. Subsequently, they were passaged independently in new confluent Vero cells in 96-well plates and maintained for additional three days at 39°C. After incubation, the number of CPE-positive wells was counted. Eventually, we confirmed the viral sequence, as described above. To confirm the risk of rTS-all reverting to the virulent phenotype *in vivo*, rTS-all and L50-33 viruses were used to infect Syrian hamsters (5 weeks, male, n = 3) at 1.8×10^5 TCID₅₀/100 μL/dose. Nasal wash specimens were collected with 500 μL of D-PBS three dpi. The viral titer in each sample was calculated as described above. To determine the genomic sequence of the virus in each sample, viral RNA was extracted and sanger sequenced as described above.

QUANTIFICATION AND STATISTICAL ANALYSIS

Each data point is expressed as the mean \pm SD or median \pm 95% CI. To analyze the viral titer in the nasal wash or lung samples, statistical analyses were performed using one-way ANOVA. For the analysis of the neutralization titer, the Kruskal-Wallis test was used to calculate statistical significance. For the analysis of the viral growth kinetics and *in vivo* weight change, two-way ANOVA was performed. For samples below the LOD, the assay's LOD was used to calculate the mean. All analyses were performed using the GraphPad Prism software (n.s.: not significant, *p < 0.05, **p < 0.01, ***p < 0.001, and ****p < 0.0001).